Topological contribution to magnetism in the Kane-Mele model: An explicit wave-function approach

Soshun Ozaki [1,*] and Masao Ogata [1,2]

[1]*Department of Physics, University of Tokyo, Bunkyo, Tokyo 113-0033, Japan*
[2]*Trans-scale Quantum Science Institute, University of Tokyo, Bunkyo, Tokyo 113-0033, Japan*

In our previous publication [Ozaki and Ogata, Phys. Rev. Res. **3**, 013058 (2021)], the quantization of the orbital-Zeeman (OZ) cross term in the magnetic susceptibility, or the cross term of spin Zeeman and orbital effect, was shown for the Kane-Mele model using the expansion around the Dirac points. In the present study, we accurately evaluate the orbital, spin-Zeeman, and OZ cross term of the Kane-Mele model using a recently developed formulation. This method uses the explicit real-space Bloch wave functions and enables us to accurately evaluate each contribution taking into account an infinite number of high-energy bands and core electron contribution at arbitrary chemical potential. We find that the effect beyond the previous formulations does not change the quantization of the OZ cross term. We also study the OZ cross term in the metalic case, and the sum rule of the OZ cross term with respect to the chemical potential is found. The possibility of experimental detection of the quantization is also discussed.

I. INTRODUCTION

Much research in recent years has focused on topological insulators (TIs) [1–14]. TIs show anomalous phenomena such as electric conduction on sample surfaces, and the search for candidate materials is one of the most important problems in this field. In particular, the novel phenomena such as spin-Hall effect and the conducting edge state robust against nonmagnetic impurities are expected in two-dimensional (2D) TIs. However, only a few materials have been confirmed to be 2D TIs [8–12]. So far, the confirmation of TI is achieved by finding the edge state in angle-resolved photoemission spectroscopy and in the transport experiments, which are both by the methods to find the anomalous edge states. Therefore, it is desirable to develop some alternative methods that detect the topological nature of a material through some observation of bulk physical quantities. One example for such quantities is the magnetic susceptibility.

Usually, the magnetic susceptibility in itinerant systems without two-body interactions is discussed in terms of the spin Zeeman effect and the orbital effect individually. Generally, however, in the system with spin-orbit interaction (SOI) the cross term of the two exists, which we call "orbital-Zeeman (OZ) cross term" in the following. The OZ cross terms were discussed for some circumstances [7,15–21]. In particular, for spin-conserving 2D TIs, the jump in the OZ term and its quantization were discussed in Refs. [7,15,21].

Nakai and Nomura [15] reported that the OZ cross term χ_{OZ} in the Bernevig-Hughes-Zhang model [5] is proportional to the spin Chern number $Ch_{s,l}$, the topological invariant for spin-conserving 2D TIs. Recently, we clarified that the coefficient of $Ch_{s,l}$ is generally given by the universal value $\chi_u = 4|e|\mu_B/h$, and confirmed the quantization in the Kane-Mele model [2,3] by using the $\boldsymbol{k} \cdot \boldsymbol{p}$ approximation explicitly [21]. This quantization is associated with the Berry curvature, and physically, it originates from the edge currents characteristic of the 2D TIs [21]. Based on these results, the magnetic susceptibility is expected to be used for the detection of the change in the topological invariant for 2D TIs. However, the evaluation for the Kane-Mele model in our previous paper was based on the effective Hamiltonian in the vicinities of K and K′ points of graphene, where the massive/massless Dirac electron system is realized. Therefore, the contributions from the distant $\boldsymbol{k}$ region from the K or K′ points or from the bands other than the two bands forming the Dirac dispersion were not evaluated accurately. Besides, the previous publication does not include some additional contributions, such as core-electron diamagnetism, the newly found Fermi surface term, and the correction term from the occupied states [22–24]. To compare the theory with experiments, it is desirable to be able to evaluate all these contributions.

It should be noted that the Kane-Mele model is based on the tight-binding model of graphene. The effect of the magnetic field is often introduced as the Peierls phase of the transfer integral in the tight-binding model. However, it is known that the Peierls phase is not enough to describe the effect of the magnetic field [25,26]. To obtain the whole magnetic susceptibility, it is necessary to use the continuum Hamiltonian with the SOI. The formulation of the orbital magnetism in such a case is not so simple owing to the complicated interband effects of the magnetic field, and a lot of efforts were dedicated [27–33]. It is notable that Fukuyama developed a one-line formula for the orbital magnetic susceptibility, which is written in terms of Green's functions [33]. (Some recent publications [34,35] proposed similar formulas.) Fukuyama's formula was reformulated in terms of Bloch wave functions with infinite summations over the band indices taken

*ozaki@hosi.phys.s.u-tokyo.ac.jp

analytically [22,36], and the resultant formula properly includes the Landau-Peierls (dia)magnetism and the contribution from occupied states, and some additional contributions. The total magnetic susceptibility is given by

$$\chi_{\text{total}} = \chi_{\text{LP}} + \chi_{\text{inter}} + \chi_{\text{FS}} + \chi_{\text{FS-P}} + \chi_{\text{occ1}} + \chi_{\text{occ2}}, \quad (1)$$

where χ_{LP}, χ_{inter}, χ_{FS}, and χ_{occ1} represent Landau-Peierls, interband, Fermi surface, and occupied state contributions, respectively. $\chi_{\text{FS-P}}$ is also the Fermi surface contribution, which contains Pauli paramagnetism. χ_{occ2} is a Berry curvature-related term. The explicit expressions for these contributions are shown in Ref. [36]. This formulation has four major advantages: (i) Since we use the completeness condition of the Bloch wave functions, we can take account of an infinite number of bands using the energy dispersions and real-space wave functions of the unperturbed bands. (ii) By using the atomic wave functions, which contain the information of atoms, we can evaluate the effect of a magnetic field on the core electrons inside the atom. (iii) We do not use effective Hamiltonians around some $\bm{k}$ points, and thus, we can evaluate contributions from the whole Brillouin zone with the correct boundaries. (iv) We can evaluate the contribution at arbitrary chemical potential. As for (iv), it should be noted that some Green's function formulations that assume a continuous periodic potential do not always give accurate chemical potential dependence when applied to tight-binding models, as discussed in Refs. [33,35]. This difficulty is conquered by this infinite-band formulation [22–24].

In this paper, we evaluate all the contributions in magnetic susceptibility including the spin Zeeman, orbital, and OZ cross term in the Kane-Mele model with silicene in mind, using the continuum Hamiltonian formulation. The real space wave functions are represented by the linear combination of atomic orbitals (LCAOs) using p_z orbitals on carbon atoms as was used in the case of simple graphene [24]. We will show that the effect beyond the tight-binding and effective-model formulations does not change or affect the quantization of the OZ cross term. We will also show that the OZ cross term has a reasonable magnitude compared with the other contributions and confirm the quantized jump at the topological phase transition. Furthermore, we study the chemical potential dependence of each contribution and find that the OZ cross term also has a large contribution at the van Hove singularity irrespective of whether the system is topological or not.

This paper is organized as follows. In Sec. II, we first review the fundamental properties of the Kane-Mele model such as the energy dispersion and topological phase diagram. Then, we derive the continuum-space Bloch wave function assuming that it consists of $2p_z$ atomic orbitals. In Sec. III, we apply the general formula for the magnetic susceptibility to the Kane-Mele model and derive analytic expressions for each contribution. In Sec. IV, we numerically evaluate the results obtained in the previous section and discuss the experimental observability of each term, especially the OZ cross term. Finally, we present the discussions and summary in Sec. V

II. EXPLICIT WAVE FUNCTIONS FOR THE KANE-MELE MODEL

We study the energy dispersion and write down the explicit wave functions for the Kane-Mele model. The tight-binding
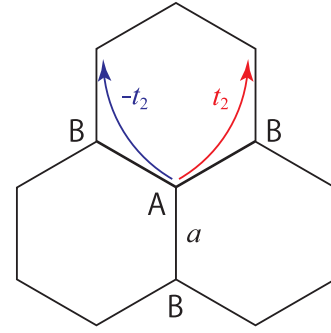

FIG. 1. Honeycomb lattice for the Kane-Mele model. A and B represent the sublattices and a is the distance between the adjacent two sites. The arrows show the hopping between the next-nearest-neighbors due to SOI. The signs of this hopping depends on the path: It is $+1(-1)$ if the electron makes a left (right) turn to propagate to a next-nearest site.

Hamiltonian is given by [2,3]

$$H = -\sum_{\langle i,j \rangle \alpha} t c_{i\alpha}^\dagger c_{j\alpha} + \Delta_0 \left(\sum_{i \in A, \alpha} c_{i\alpha}^\dagger c_{i\alpha} - \sum_{i \in B, \alpha} c_{i\alpha}^\dagger c_{i\alpha} \right)$$
$$+ \sum_{\langle\langle i,j \rangle\rangle, \alpha, \beta} it_2 v_{ij} c_{i\alpha}^\dagger \sigma_{\alpha\beta}^z c_{j\beta}, \quad (2)$$

where $c_{i\alpha}^\dagger$ creates an electron with spin α at site i, and $\langle i, j \rangle$ ($\langle\langle i, j \rangle\rangle$) run over all the nearest- (next-nearest-)neighbor sites of a two-dimensional honeycomb lattice defined in Fig. 1. The first term represents usual nearest-neighbor hoppings with transfer integral t. The second term represents a staggered on-site potential, $+\Delta_0$ for the sites in the A sublattice and $-\Delta_0$ for those in the B sublattice. The summation $\sum_{i\in A}$ ($\sum_{i\in B}$) means the sum over the sites in the A (B) sublattice. The last term represents the hopping between the next-nearest-neighbor sites due to SOI, where $\sigma_{\alpha\beta}^z$ is the $(\alpha\beta)$ component of the spin operator in the z direction, and $v_{ij} = -v_{ji} = +1$ (−1) if the electron makes a left (right) turn to propagate to a next-nearest site (see Fig. 1). Only the σ^z component of SOI appears [3,37,38], whose microscopic derivation using the LACOs is shown in Appendix A. This model is known as the model for silicene [37–41]. Silicene has a backled structure, and A and B sublattices are not located on the same 2D plane. Therefore, when an electric field is applied perpendicularly to the 2D plane, the difference in height gives rise to the staggered potential Δ_0. For the next-nearest-neighbor hoppings, we focus on t_2 in Eq. (2), since it plays an important role in the topological phase transition even if it is small [21,37,38]. Generally, there will be spin conserving next-nearest neighbor hoppings. However, we consider that they only modify the energy dispersion and they do not lead to the topological phase transition.

As discussed in Sec. I, to include all the effect of a magnetic field correctly, we consider the Hamiltonian in the continuum space,

$$H^{\text{full}} = \frac{1}{2m}(\bm{p} - e\bm{A})^2 + V(\bm{r}) + \frac{\hbar^2}{8m^2c^2}\nabla^2 V$$
$$+ \frac{\hbar}{4m^2c^2}\bm{\sigma} \cdot \nabla V \times (\bm{p} - e\bm{A}) - \frac{e\hbar}{2m}\bm{\sigma} \cdot \bm{B}, \quad (3)$$

where $e(< 0)$ is the electron charge, $A(r)$ is a vector potential ($B = \mathrm{rot}A$). $V(r)$ is the periodic potential that represents the honeycomb lattice and the fourth term represents the SOI derived from the relativistic Dirac equation. Once $V(r)$ is fixed, t, Δ_0, and t_2 are determined simultaneously. However, in our calculations, we treat t, Δ_0, and t_2 as variable parameters. The changes in the parameters should be interpreted as the changes in the functional form of $V(r)$. We have set the g factor in the last term (spin Zeeman term) to be $g = 2$ neglecting the QED corrections. When we consider a tight-binding model under a magnetic field, a renormalization of the g factor generally occurs owing to the virtual interband process [42,43], and the effective g factor deviates from $g = 2$ in the focused bands. However, since the Hamiltonian Eq. (3) contains all the bands, the Zeeman term in Eq. (3) should have the bare g factor, $g = 2$. At the end of calculation including the interband processes, the effective g factor should naturally appear.

We apply Eq. (3) to the Kane-Mele model. In Eq. (3), $V(r)$ is chosen to be the periodic potential formed by the atoms on the honeycomb lattice,

$$V(r) = \sum_{i \in A} V_A(r - R_{Ai}) + \sum_{i \in B} V_B(r - R_{Bi}), \quad (4)$$

where R_{Ai} (R_{Bi}) represents the position of the site in the A (B) sublattice in the ith unit cell. For the continuum Hamiltonian Eq. (3), we write down the Bloch wave functions in terms of LCAOs of the A and B sublattice [24], assuming that the wave functions near the Fermi level consist of $2p_z$ orbitals. Then, the wave functions are expressed as the linear combinations of the orthogonal wave functions localized at a site $r = R_i$. (The other bands are treated later.) As a simple case, we use $2p_z$ orbital,

$$\phi_{2p_z}(r) = \frac{1}{\sqrt{24}(a_B^*)^{5/2}} \sqrt{\frac{3}{4\pi}} z e^{-r/2a_B^*}, \quad (5)$$

where $a_B^* = a_B/Z_{\mathrm{eff}}$ is the renormalized Bohr radius, $a_B = \hbar^2/me^2$ is the Bohr radius, and $Z_{\mathrm{eff}} = 3.25$ [24,44] is the effective charge of carbon atoms. The orthogonal localized basis is given by [23–25]

$$\Phi(r - R_i) = \phi_{2p_z}(r - R_i) - \sum_{j: \mathrm{n.n.}} \frac{s}{2} \phi_{2p_z}(r - R_j). \quad (6)$$

In Eq. (6), j summation is taken over the nearest-neighbor (n.n.) sites of R_i, and s is the overlap integral between the adjacent sites,

$$s = \int \phi_{2p_z}^*(r - R_i) \phi_{2p_z}(r - R_j) dr. \quad (7)$$

The orthogonality of $\Phi(r - R_i)$ is maintained up to the first order with respect to s. Note that s is independent of the direction $R = R_j - R_i$ since the p_z orbital is isotropic in the xy plane.

Next, we perform a Fourier transform and obtain the basis

$$\varphi_{Ak}(r) = \frac{1}{\sqrt{N}} \sum_{R_{Ai}} e^{-ik(r-R_{Ai})} \Phi(r - R_{Ai}) \quad (8)$$

and

$$\varphi_{Bk}(r) = \frac{1}{\sqrt{N}} \sum_{R_{Bi}} e^{-ik(r-R_{Bi})} \Phi(r - R_{Bi}), \quad (9)$$

where N is the total number of sites on each sublattice. The periodic part of the Bloch wave function $u_{lk\sigma}(r)$ is determined by the eigenvalue equation,

$$H_{k\sigma} u_{lk\sigma} = E_{lk\sigma} u_{lk\sigma}, \quad H_{k\sigma} = e^{-ikr} H^{\mathrm{full}} e^{ikr}, \quad (10)$$

where l and $\sigma (= \pm 1)$ represent the band index and the eigenvalue of the z component of spin of an electron: $\sigma = 1$ for spin-up and $\sigma = -1$ for spin-down. We denote the two energy dispersion and the two eigenfunctions near the Fermi level as $E_{k\sigma}^\pm$ and $u_{k\sigma}^\pm(r)$, respectively. To determine $E_{k\sigma}^\pm$ and $u_{k\sigma}^\pm(r)$, we calculate the matrix elements of the Hamiltonian $H_{k\sigma}$ in terms of the obtained basis,

$$h_{nm\sigma}(k) = \int \varphi_{nk}^*(r) H_{k\sigma} \varphi_{mk}(r) dr, \quad (11)$$

with $n, m =$ A or B. They become

$$h_{AA\sigma} = \Delta_{k\sigma} + E_0, \quad (12)$$

$$h_{BB\sigma} = -\Delta_{k\sigma} + E_0, \quad (13)$$

$$h_{AB\sigma} = h_{BA\sigma}^* = -t\gamma_k, \quad (14)$$

where E_0 is the energy constant [24],

$$\Delta_{k\sigma} = \Delta_0 + 4\sigma t_2 \sin \frac{\sqrt{3}}{2} k_x a \left(\cos \frac{3}{2} k_y a - \cos \frac{\sqrt{3}}{2} k_x a \right) \quad (15)$$

and

$$\gamma_k = e^{-ik_y a} + e^{i(\frac{\sqrt{3}}{2} k_x + \frac{1}{2} k_y)a} + e^{i(-\frac{\sqrt{3}}{2} k_x + \frac{1}{2} k_y)a}, \quad (16)$$

with a being the distance between the nearest-neighbor sites. Hereafter, we set $E_0 = 0$ without loss of generality. Δ_0 corresponds to the staggered on-site potential in Eq. (2) and the nearest-neighbor hopping t can be expressed as a kind of overlap integral [24]. As shown in Appendix A, the SOI in Eq. (3) does not give contributions to the nearest-neighbor hopping, but it leads to a next-nearest-neighbor hopping t_2 in Eq. (2), which is also expressed by a kind of the overlap integrals. In Appendix A, it is also shown that the next-nearest-neighbor hopping have only the z component of spin $\sigma_{\sigma\sigma'}^z$; therefore, the spin is conserved.

By diagonalizing the Hamiltonian $h_{nm\sigma}(k)$, we obtain the energy dispersion,

$$E_{k\sigma}^\pm = \pm \sqrt{\Delta_{k\sigma}^2 + \varepsilon_k^2}, \quad (17)$$

where $\varepsilon_k := t|\gamma_k|$. At K $= (4\pi/3\sqrt{3}a, 0)$ and K$' = (-4\pi/3\sqrt{3}a, 0)$ in the Brillouin zone, γ_k vanishes. Figure 2(a) shows the energy dispersions Eq. (17) with $\sigma = +1$ (up spin) [21]. The solid and the dashed lines
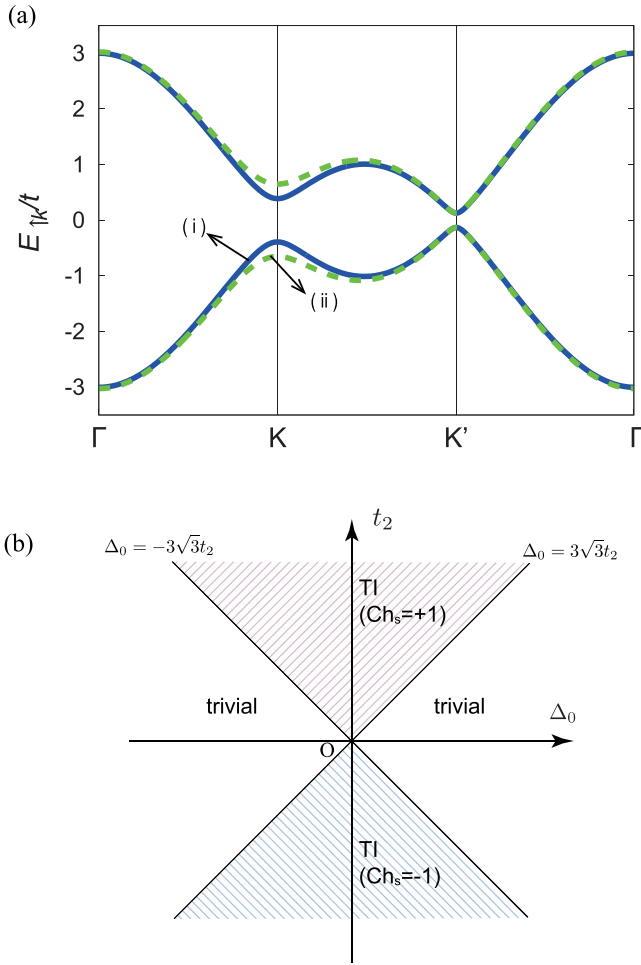
(a)

(b)

FIG. 2. (a) Energy dispersion of Eq. (2) for $\sigma = 1$ (up spin) along the path $\Gamma \to K \to K' \to \Gamma$ for two typical choices of parameters: (i) solid line, $\Delta_0/t = 1/4$, $t_2/t = \sqrt{3}/72$ (topologically trivial) and (ii) dashed line, $\Delta_0/t = 1/4$, $t_2/t = \sqrt{3}/24$ (topologically nontrivial). The energy dispersion for $\sigma = -1$ (down spin) is obtained by exchanging K for K' points. (b) Phase diagram of the present model. The shaded areas represent topologically nontrivial paramter regions.

in Fig. 2 are for the cases of $\Delta_0/t = 1/4$, $t_2/t = \sqrt{3}/72$ (topologically trivial) and $\Delta_0/t = 1/4$, $t_2/t = \sqrt{3}/24$ (topologically nontrivial), respectively. The dispersions are similar to those of graphene but gaps open at K and K'

points. The magnitudes of the gaps at K and K' points are given by

$$2|\Delta_0 + 3\sqrt{3}\sigma t_2|, \quad 2|\Delta_0 - 3\sqrt{3}\sigma t_2|, \quad (18)$$

respectively. Owing to the SOI, the energy dispersions for spin-up and spin-down are not the same. The energy dispersion for $\sigma = -1$ (down spin) is obtained by exchanging K for K' points in Fig. 2. Figure 2(b) shows the phase diagram of the model Eq. (2). The system is topologically trivial for $|\Delta_0| > 3\sqrt{3}|t_2|$ while the system is topologically nontrivial for $|\Delta_0| < 3\sqrt{3}|t_2|$. As usual, the gap closes at the nontrivial-trivial critical points, $\Delta_0 = \pm 3\sqrt{3}t_2$.

The two eigenfunctions, $u_{k\sigma}^{\pm}(r)$, are obtained as

$$u_{k\sigma}^+(r) = e^{\frac{i}{2}\theta_k} \cos \eta_{k\sigma} \varphi_{Ak}(r) - e^{-\frac{i}{2}\theta_k} \sin \eta_{k\sigma} \varphi_{Bk}(r) \quad (19)$$

and

$$u_{k\sigma}^-(r) = e^{\frac{i}{2}\theta_k} \sin \eta_{k\sigma} \varphi_{Ak}(r) + e^{-\frac{i}{2}\theta_k} \cos \eta_{k\sigma} \varphi_{Bk}(r), \quad (20)$$

where

$$e^{i\theta_k} = \frac{\gamma_k}{|\gamma_k|}, \quad (21)$$

$$\cos \eta_{k\sigma} = \sqrt{\frac{1}{2}\left(1 + \frac{\Delta_{k\sigma}}{|E_{k\sigma}^{\pm}|}\right)}, \quad (22)$$

$$\sin \eta_{k\sigma} = \sqrt{\frac{1}{2}\left(1 - \frac{\Delta_{k\sigma}}{|E_{k\sigma}^{\pm}|}\right)}. \quad (23)$$

If we set $\eta_{k\sigma} = \frac{\pi}{4}$, then these eigenfunctions coincide with those for (massless) graphene [24].

Note that the Hamiltonian Eq. (3) contains all the bands. In the following, the eigenenergies and eigenfunctions of all the other bands are denoted as $E_{l'k\sigma}$ and $u_{l'k\sigma}(r)$ with $l' \neq \pm$. As we will show later, they are used in the interband contribution of magnetic susceptibility χ_{inter}, but the explicit forms of $E_{l'k\sigma}$ and $u_{l'k\sigma}(r)$ are not necessary.

III. MAGNETIC SUSCEPTIBILITY

Generally, the magnetic susceptibility consists of six contributions shown in Eq. (1) [22,36]. Using the eigenenergies and eigenfunctions mentioned above, each term in Eq. (1) becomes

$$\chi_{\text{LP}} = \frac{e^2}{12\hbar^2} \sum_{\pm, k\sigma} f'(E_{k\sigma}^{\pm}) \left[\frac{\partial^2 E_{k\sigma}^{\pm}}{\partial k_x^2} \frac{\partial^2 E_{k\sigma}^{\pm}}{\partial k_y^2} - \left(\frac{\partial^2 E_{k\sigma}^{\pm}}{\partial k_x \partial k_y} \right)^2 \right], \quad (24)$$

$$\chi_{\text{inter}} = -2 \sum_{\pm} \sum_{l' \neq \pm, \mp,} \sum_{k,\sigma} \frac{f(E_{k\sigma}^{\pm})}{E_{k\sigma}^{\pm} - E_{l'k\sigma}} |M_{\pm l'\sigma}|^2, \quad (25)$$

$$\chi_{\text{FS}} = \frac{e^2}{2\hbar^2} \text{Re} \sum_{\pm, k, \sigma} f'(E_{k\sigma}^{\pm}) \left[\left\{ \frac{\partial E_{k\sigma}^{\pm}}{\partial k_x} \int \frac{\partial u_{k\sigma}^{\pm *}}{\partial k_y} \left(\frac{\partial H_k}{\partial k_x} + \frac{\partial E_{k\sigma}^{\pm}}{\partial k_x} \right) \frac{\partial u_{k\sigma}^{\pm}}{\partial k_y} dr \right. \right.$$

$$\left. \left. - \frac{\partial E_{k\sigma}^{\pm}}{\partial k_x} \int \frac{\partial u_{k\sigma}^{\pm *}}{\partial k_x} \left(\frac{\partial H_k}{\partial k_y} + \frac{\partial E_{k\sigma}^{\pm}}{\partial k_y} \right) \frac{\partial u_{k\sigma}^{\pm}}{\partial k_y} dr + (x \leftrightarrow y) \right\} - \left\{ \frac{i\hbar^2}{m} \frac{\partial E_{k\sigma}^{\pm}}{\partial k_x} \int u_{k\sigma}^{\pm *} \sigma_z \frac{\partial u_{k\sigma}^{\pm}}{\partial k_y} dr - (x \leftrightarrow y) \right\} \right], \quad (26)$$

$$\chi_{\text{FS}-\text{P}} = -\sum_{\pm,\boldsymbol{k},\sigma} f'(E_{\boldsymbol{k}\sigma}^{\pm})|M_{\pm\pm\sigma}|^2, \tag{27}$$

$$\chi_{\text{occ1}} = -\frac{e^2}{4\hbar^2} \sum_{\pm,\boldsymbol{k},\sigma} f(E_{\boldsymbol{k}\sigma}^{\pm}) \left[\frac{\partial^2 E_{\boldsymbol{k}\sigma}^{\pm}}{\partial k_x \partial k_y} \int \frac{\partial u_{\boldsymbol{k}\sigma}^{\pm*}}{\partial k_x} \frac{\partial u_{\boldsymbol{k}\sigma}^{\pm}}{\partial k_y} d\boldsymbol{r} + \left(\frac{\hbar^2}{m} - \frac{\partial^2 E_{\boldsymbol{k}\sigma}^{\pm}}{\partial k_x^2} \right) \int \frac{\partial u_{\boldsymbol{k}\sigma}^{\pm*}}{\partial k_y} \frac{\partial u_{\boldsymbol{k}\sigma}^{\pm}}{\partial k_y} d\boldsymbol{r} \right] + (x \leftrightarrow y), \tag{28}$$

$$\chi_{\text{occ2}} = -\frac{e}{\hbar} \text{Re} \sum_{\pm,\boldsymbol{k},\sigma} f(E_{\boldsymbol{k}\sigma}^{\pm}) M_{\pm\pm\sigma} \Omega_{\pm\sigma}, \tag{29}$$

where $M_{ll'\sigma}$ is the magnetic moment defined by

$$M_{ll'\sigma} = -\frac{ie}{2\hbar} \left\{ \int \frac{\partial u_{l\boldsymbol{k}\sigma}^*}{\partial k_x} \left(\frac{\partial H_{\boldsymbol{k}}}{\partial k_y} + \frac{\partial E_{l\boldsymbol{k}\sigma}}{\partial k_y} \right) u_{l'\boldsymbol{k}\sigma} d\boldsymbol{r} \right.$$
$$\left. - \int \frac{\partial u_{l\boldsymbol{k}\sigma}^*}{\partial k_y} \left(\frac{\partial H_{\boldsymbol{k}}}{\partial k_x} + \frac{\partial E_{l\boldsymbol{k}\sigma}}{\partial k_x} \right) u_{l'\boldsymbol{k}\sigma} d\boldsymbol{r} \right\}$$
$$+ \frac{e\hbar}{2m} \int u_{l\boldsymbol{k}\sigma}^* \sigma_z u_{l'\boldsymbol{k}\sigma} d\boldsymbol{r}, \tag{30}$$

and $\Omega_{\pm\sigma}$ is the z component of the Berry curvature

$$\Omega_{\pm\sigma} = i \int d\boldsymbol{r} \left(\frac{\partial u_{\boldsymbol{k}\sigma}^{\pm*}}{\partial k_x} \frac{\partial u_{\boldsymbol{k}\sigma}^{\pm}}{\partial k_y} - \frac{\partial u_{\boldsymbol{k}\sigma}^{\pm*}}{\partial k_y} \frac{\partial u_{\boldsymbol{k}\sigma}^{\pm}}{\partial k_x} \right). \tag{31}$$

In principle, there are contributions of core level electrons (i.e., in the $1s$ orbital, etc.) in χ_{occ1} and χ_{occ2}, which we do not consider in the following.

Various integrals appearing in the above equations are calculated by using the Bloch wave functions in Eqs. (19) and (20) up to the first order with respect to the "overlap integrals" s, t, and t_2, whose integrands contain the overlap of atomic orbitals $\phi_{2p_z}^*(\boldsymbol{r} - \boldsymbol{R}_j)\phi_{2p_z}(\boldsymbol{r} - \boldsymbol{R}_i)$, with $\boldsymbol{R}_i$ and $\boldsymbol{R}_j$ being the nearest-neighbor sites or next-nearest-neighbor sites. The obtained integrals are shown in Appendix B. In the following, we write $E_{\boldsymbol{k}\sigma} := \sqrt{\Delta_{\boldsymbol{k}\sigma}^2 + \varepsilon_{\boldsymbol{k}}^2}$ (i.e., $E_{\boldsymbol{k}\sigma}^{\pm} = \pm E_{\boldsymbol{k}\sigma}$). Furthermore, to simplify the expressions we abbreviate $\varepsilon_{\boldsymbol{k}}$, $\theta_{\boldsymbol{k}}$, $E_{\boldsymbol{k}\sigma}$, $\Delta_{\boldsymbol{k}\sigma}$, and $\eta_{\boldsymbol{k}\sigma}$ as ε, θ, E, Δ, and η, respectively, as long as they do not cause ambiguity. We also use the abbreviations

$$\varepsilon_\mu = \frac{\partial \varepsilon}{\partial k_\mu}, \quad \theta_\mu = \frac{\partial \theta}{\partial k_\mu}, \quad E_\mu = \frac{\partial E}{\partial k_\mu}, \quad \Delta_\mu = \frac{\partial \Delta}{\partial k_\mu},$$

$$\eta_\mu = \frac{\partial \eta}{\partial k_\mu}, \quad \varepsilon_{\mu\nu} = \frac{\partial^2 \varepsilon}{\partial k_\mu \partial k_\nu}, \quad \theta_{\mu\nu} = \frac{\partial^2 \theta}{\partial k_\mu \partial k_\nu}, \tag{32}$$

$$E_{\mu\nu} = \frac{\partial^2 E}{\partial k_\mu \partial k_\nu}, \quad \Delta_{\mu\nu} = \frac{\partial^2 \Delta}{\partial k_\mu \partial k_\nu}, \quad \eta_{\mu\nu} = \frac{\partial^2 \eta}{\partial k_\mu \partial k_\nu},$$

for μ, $\nu = x$ or y. For example, using the formula (F3) in Appendix B, we obtain the Berry curvature as

$$\Omega_{\pm\sigma} = \mp \frac{\varepsilon}{E} (\theta_x \eta_y - \theta_y \eta_x) + O(s^2), \tag{33}$$

However, using the formulas (F1) and (F7) in Appendix B, the diagonal matrix element of magnetic moment $M_{\pm\pm\sigma}$ becomes

$$M_{\pm\pm\sigma} = \frac{e}{2\hbar} (\Delta_x \theta_y - \Delta_y \theta_x) + \frac{e\hbar}{2m} \sigma + O(s^2). \tag{34}$$

Here we have used the relation

$$\frac{\Delta}{E} E_\mu - 2\varepsilon \eta_\mu = \Delta_\mu, \tag{35}$$

which is shown in Appendix C. Other useful relations are also shown in Appendix C.

From the explicit forms of E, $\Omega_{\pm\sigma}$, and $M_{\pm\pm\sigma}$, it is straightforward to write down χ_{LP}, $\chi_{\text{FS}-\text{P}}$, and χ_{occ2}. χ_{FS} and χ_{occ1} are shown in Appendix D, where we have used the integral formulas in Appendix B. χ_{inter} contains the summation over $E_{l'\boldsymbol{k}\sigma}$ and $u_{l'\boldsymbol{k}\sigma}$, which are the other energy dispersions and wave functions than for the two bands forming the Dirac dispersion. We can calculate the summation over l' without using the explicit expression of $u_{l'\boldsymbol{k}\sigma}$ by making use of the completeness condition,

$$u_{\boldsymbol{k}\sigma}^+(\boldsymbol{r}) u_{\boldsymbol{k}\sigma}^{+*}(\boldsymbol{r}') + u_{\boldsymbol{k}\sigma}^-(\boldsymbol{r}) u_{\boldsymbol{k}\sigma}^{-*}(\boldsymbol{r}') + \sum_{l' \neq \pm, \sigma} u_{l'\boldsymbol{k}\sigma}(\boldsymbol{r}) u_{l'\boldsymbol{k}\sigma}^*(\boldsymbol{r}')$$
$$= \delta(\boldsymbol{r} - \boldsymbol{r}'). \tag{36}$$

The details of calculations are shown in Appendix E.

χ_{total} [Eq. (1)] is calculated in Appendix D, which is classified into a few groups as follows:

$$\chi_{\text{total}} = \chi_{\text{LP}} + \chi_{\text{Pauli}} + \chi_{\text{OZ}} + \chi_{\text{atomic}} + \chi_1 + \chi_2, \tag{37}$$

with

$$\chi_{\text{LP}} = \frac{e^2}{12\hbar^2} \sum_{\pm,\boldsymbol{k}\sigma} f'(\pm E) \left[E_{xx} E_{yy} - E_{xy}^2 \right], \tag{38}$$

$$\chi_{\text{Pauli}} = -\frac{e^2 \hbar^2}{4m^2} \sum_{\pm,\boldsymbol{k}\sigma} f'(\pm E), \tag{39}$$

$$\chi_{\text{OZ}} = \frac{e^2}{m} \sum_{\pm,\boldsymbol{k},\sigma} f'(\pm E) \sigma \varepsilon (\eta_x \theta_y - \eta_y \theta_x) - \frac{e^2}{m} \sum_{\pm,\boldsymbol{k},\sigma} f(\pm E) \sigma \Omega_{\pm\sigma} + O(s^2), \tag{40}$$

$$\chi_{\text{atomic}} = -\frac{e^2}{4m} \sum_{\pm,\boldsymbol{k},\sigma} f(\pm E) \langle x^2 + y^2 \rangle = -\frac{3e^2 a_{\text{B}}^{*2}}{m} n(\mu) + O(s^2), \tag{41}$$

$$\chi_1 = \frac{e^2}{\hbar^2} \sum_{\pm,\bm{k},\sigma} f(\pm E) \Bigg[\pm \frac{\eta_x^2}{2E}(\varepsilon\varepsilon_{yy} + \Delta\Delta_{yy}) \mp \frac{\eta_x\eta_y}{2E}(\varepsilon\varepsilon_{xy} + \Delta\Delta_{xy}) \mp \frac{\varepsilon\Delta}{4E}(\eta_x\theta_x\theta_{yy} - \eta_x\theta_y\theta_{xy})$$

$$\pm \frac{1}{8}(E_x\theta_x\theta_{yy} - E_x\theta_y\theta_{xy}) \mp \frac{\theta_x^2}{8E}(\Delta\Delta_{yy} + 2\varepsilon\Delta_y\eta_y) \pm \frac{\theta_x\theta_y}{8E}(\Delta\Delta_{xy} + 2\varepsilon\Delta_x\eta_y)\Bigg] + (x \leftrightarrow y)$$

$$+ \frac{e^2}{\hbar^2}\sum_{\pm k\sigma} f'(\pm E)\Bigg[\frac{\varepsilon^2 E_x}{8E}(\theta_y\theta_{xy} - \theta_x\theta_{yy}) + \frac{\Delta E_x}{8E}(\Delta_x\theta_y^2 - \Delta_y\theta_x\theta_y)$$

$$+ \frac{E_x}{4E}\{\eta_y(\Delta\varepsilon_{xy} - \varepsilon\Delta_{xy}) - \eta_x(\Delta\varepsilon_{yy} - \varepsilon\Delta_{yy})\} - \frac{1}{4}\big(\theta_x^2\Delta_y^2 - \theta_x\theta_y\Delta_x\Delta_y\big)\Bigg] + (x \leftrightarrow y) + O(s^2), \tag{42}$$

$$\chi_2 = \frac{e^2}{\hbar^2}\sum_{\pm,\bm{k},\sigma} f(\pm E)\Bigg[\mp \frac{\langle y^2 \rangle}{4E}(-a^2\varepsilon^2 + \Delta\Delta_{xx} + \Delta\Delta_{yy}) \mp \frac{\hbar^2}{4m}\bigg(\frac{a^2 s\varepsilon^2}{2Et} - \frac{\varepsilon^2}{Et}\langle x^2 + y^2 \rangle_R\bigg)\Bigg] + O(s^2). \tag{43}$$

The "expectation values" $\langle\cdots\rangle$ and $\langle\cdots\rangle_R$ are defined by

$$\langle x^2 + y^2 \rangle = \int \Phi^*(\bm{r})(x^2 + y^2)\Phi(\bm{r})d\bm{r} \tag{44}$$

and

$$\langle x^2 + y^2 \rangle_R = \int \Phi^*(\bm{r} - \bm{R})(x^2 + y^2)\Phi(\bm{r})d\bm{r}, \tag{45}$$

with $\bm{R}$ being one of the vectors that point adjacent sites. Note that the value $\langle x^2 + y^2 \rangle_R$ depends on $R = |\bm{R}|$, and does not depend on the direction of $\bm{R}$. The present result is consistent with the previous one for graphene [24], but there appear several new contributions due to the presence of the staggered on-site potential Δ_0 and SOI t_2.

χ_{Pauli} is the Pauli paramagnetism and χ_{OZ} is the OZ cross term. Note that the χ_{OZ} should be proportional to $\mu_{\text{B}}\sigma$, since it is the cross term of the vector potential and the Zeeman term. The formula obtained in the previous paper [21] gives the same result as Eq. (40) as shown in Appendix D. The orbital contributions are classified in χ_{LP}, χ_{atomic}, χ_1, and χ_2. χ_{atomic} and χ_2 represent the zeroth order terms with respect to the transfer integral t and t_2, i.e., proportional to t^0 or $(t_2)^0$, while χ_{LP} and χ_1 are the first order terms proportional to t or t_2. χ_{atomic} represents the contributions from the occupied states in the partially filled $2p_z$-band, which we call "intraband atomic diamagnetism" [22–24]. $n(\mu)$ in χ_{atomic} represents the total electron number with spin considered when the chemical potential is μ. Since χ_2 is not proportional to t or t_2 it corresponds to the contribution not related to the Peierls phase. Instead, χ_2 includes the corrections of χ_{atomic} and the effect of the overlap integral, s. However, χ_1 is in the same order as χ_{LP}, and it represents another pure orbital contribution. Note that in the absence of the SOI, $\Delta_x = \Delta_y = \Delta_{xx} = \Delta_{yy} = \Delta_{xy} = 0$, so that χ_1 and χ_2 become simple.

IV. NUMERICAL RESULTS

A. Chemical potential dependence

Performing the numerical integration for the $\bm{k}$-summation, we obtain the magnetic susceptibility. The parameters used are taken from the values in graphene, which are tabulated in Table I [24]. Figure 3 shows each contribution to magnetic susceptibility for some choices of parameters,

$\{\Delta_0, t_2\}$: (a) $\{\Delta_0/t, t_2/t\} = \{1/2, 0\}$, (b) $\{1/4, \sqrt{3}/72\}$, and (c) $\{1/4, \sqrt{3}/24\}$ as functions of chemical potential. In each figure, the classified contributions are shown. The left figures show χ_{LP} (red, solid line), χ_1 (blue, dashed line), and χ_2 (green, dot-dashed line). The middle figures show χ_{OZ} (red, solid line), χ_{atomic} (blue, dashed line), and χ_{Pauli} (green, dot-dashed line). The right figures show the total contribution χ_{total}. The values are shown in units of $\chi_0 = e^2L^2a^2t/(2\pi\hbar)^2$. There are several remarks on the above results.

(i) For $t_2 = 0$ case [Fig. 3(a)], $\chi_{\text{LP}} + \chi_1$ coincides with the result by Raoux et al. [35], which is based on the Peierls-phase formulation. The present result has additional contributions, χ_{Pauli}, χ_2, and χ_{atomic}. Figure 4 shows $\chi_{\text{LP}} + \chi_1$ (i.e., the result by Raoux et al.; red, solid line), χ_{Pauli} (blue, dahsed line), and $\chi_2 + \chi_{\text{atomic}}$ (green, dot-dashed line). $\chi_2 + \chi_{\text{atomic}}$ originates from the deformation of the wave functions [22–24,26], which is not considered in the Peierls-phase formulation. This effect also exists for finite t_2 cases. Note that χ_{OZ} vanishes in this case.

(ii) The term χ_{atomic} in Eq. (41) is in the zeroth order with respect to the overlap integrals as in the square lattice and graphene cases [23,24]. This term is proportional to the electron number of $2p_z$ band, $n(\mu)$. Since this originates from the motion of an electron in an atom, this term does not depend on the magnitude of the overlap integral or the amplitude of transfer integral. This term produces asymmetric dependence on μ.

(iii) At the band bottom ($\mu \simeq -\sqrt{9t^2 + \Delta_0^2}$), only χ_{LP} and χ_{Pauli} have contributions. The former represents the Landau-Peierls diamagnetism [27,28], which is understood as the extension of Landau's diamagnetism for a periodic system; The

TABLE I. Parameters for graphene that are used in the numerical integration [24].

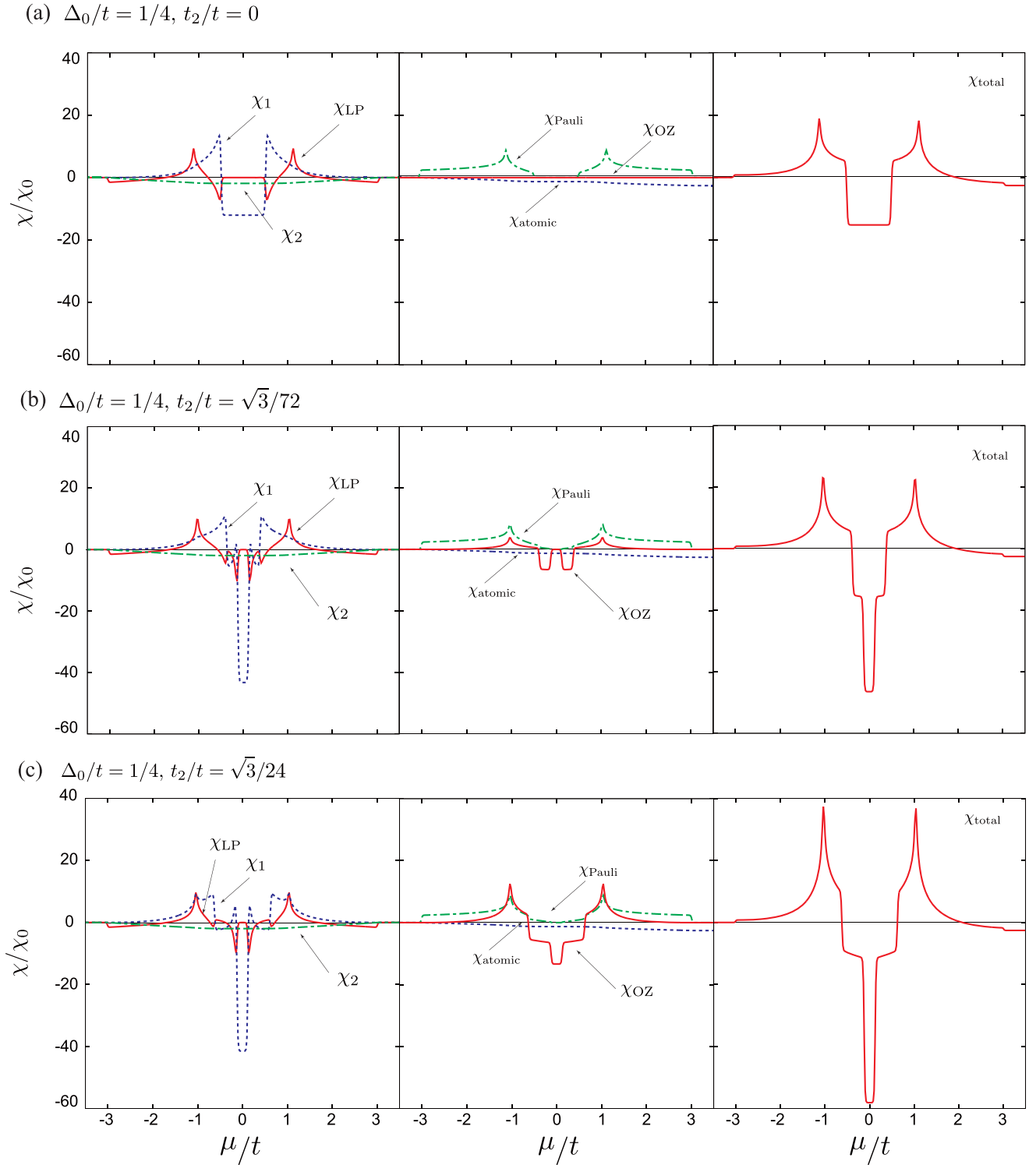| Parameters	Value
a	1.42
s	0.237
t	3.55
Z_{eff}	3.25

FIG. 3. Each contributions to the magnetic susceptibility as a function of the chemical potential. Left: χ_{LP} (red, solid line), χ_1 (blue, dashed line), and χ_2 (green, dot-dashed line). Middle: χ_{OZ} (red, solid line), χ_{atomic} (blue, dashed line), and χ_{Pauli} (green, dot-dashed line). Right: figures show the total contribution χ_{total}.

latter represents Pauli paramagnetism, the magnitude of which is proportional to the density of states. The ratio of these contribution is given by $|\chi_{\mathrm{LP}}/\chi_{\mathrm{Pauli}}| = \frac{1}{3}(m/m^*)^2$ where m^* is the effective mass at the band bottom [45]. For $\Delta_0 = 0$ case, $m^* = 2\hbar^2/3ta$ [24] and the ratio becomes $|\chi_{\mathrm{LP}}/\chi_{\mathrm{Pauli}}| = 0.659$

with the parameters shown in Table I. Thus the total magnetic susceptibility is paramagnetic at the band bottom.

(iv) At the van Hove singularity ($\mu \simeq \pm t$), we observe sharp peaks in χ_{LP}, χ_{Pauli}, and χ_{OZ}. This fact suggests that χ_{OZ} is not just a small correction to the magnetic susceptibility,
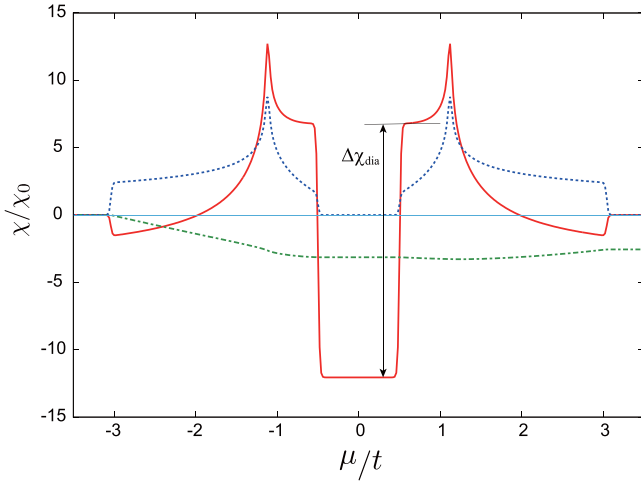
FIG. 4. Contributions to magnetic susceptibility as a function of the chemical potential at $\Delta_0 = 0.5t$ and $t_2 = 0$. The solid (red), dashed (blue), and dot-dashed (green) lines correspond to $\chi_1 + \chi_{\rm LP}$ (i.e., the result by Raoux *et al.*), $\chi_{\rm Pauli}$, and χ_2, respectively. The jump at the both ends of gap in $\chi_1 + \chi_{\rm LP}$ is denoted as $\Delta\chi_{\rm dia}$.

but one of the major contributions. The term $\chi_{\rm OZ}$ exists when $t_2 \neq 0$ and reflects the sign of t_2, and its peak at the van Hove singularity becomes negative for $t_2 < 0$. The behavior of the OZ cross term and other contributions for some extended parameters are shown in Appendix F.

(v) In $\chi_{\rm total}$ near $\mu = 0$ shown in Figs. 3(a)–3(c), we find one plateau for $t_2 = 0$ and two plateaus for finite t_2. These behaviors are explained as follows. First, the effective Hamiltonian in the vicinities of K and K′ points is given by

$$H_{\rm eff} = \hbar v k_x \tau_x + \hbar v k_y \tau_y + m_0 \tau_z, \qquad (46)$$

where $v = 3ta/2\hbar$ is velocity and $m_0 = |\Delta_0 + 3\sqrt{3}\sigma t_2|$ ($|\Delta_0 - 3\sqrt{3}\sigma t_2|$) for K (K′) point. For this system, the orbital magnetic susceptibility with chemical potential μ is obtained as [35]

$$\chi_{\rm 2DDirac}(\mu, T, m_0) = \frac{3\pi t}{2|m_0|}[f(|m_0|) - f(-|m_0|)]\chi_0, \qquad (47)$$

$$= -\frac{3\pi t}{2|m_0|}\chi_0 \theta(|m_0| - |\mu|) \ (T = 0). \qquad (48)$$

This equation shows that $\chi_{\rm 2DDirac}(\mu, T = 0, \Delta_0)$ has a finite negative value only when μ is in the gap. For finite t_2 cases, gaps of different sizes open at K and K′ points, and thus, the multiplateau structure is formed.

(vi) For the case of $t_2 = \sqrt{3}/24$ [Fig. 3(c)], apart from the contribution discussed in (v), we observe an extra diamagnetic contribution $\chi_{\rm OZ}$ at $\mu = 0$. This condition corresponds to the topologically nontrivial state, and $\chi_{\rm OZ}$ reflects the topological invariant of the model, the spin Chern number [46]. Note that the sign of $\chi_{\rm OZ}$ depends on t_2, and $\chi_{\rm OZ}$ is not always diamagnetic. In Sec. IV C, we discuss the relation in detail.

(vii) The orbital magnetic susceptibility, apart from the contribution from the core electrons and effect of overlap integral, satisfies a sum rule over the chemical potential [34,35,47–49]. We show that the sum rule also applies to $\chi_{\rm OZ}$ at $T = 0$. The integral of the second term of Eq. (40) is

calculated as

$$\int_{-\infty}^{\infty} d\mu \left(-\frac{e^2}{m}\right) \sum_{\pm k\sigma} f(\pm E) \sigma \Omega_{\pm\sigma}$$

$$= -\frac{e^2}{m} \sum_{k\sigma} \int_{-\infty}^{\infty} d\mu [\theta(\mu + E) - \theta(\mu - E)]\sigma \Omega_{-,\sigma}$$

$$= -\frac{e^2}{m} \sum_{k\sigma} \sigma \cdot 2E \Omega_{-,\sigma}$$

$$= -\frac{2e^2}{m} \sum_{k\sigma} \sigma \varepsilon(\theta_x \eta_y - \theta_y \eta_x). \qquad (49)$$

However, the integral of the first term is calculated with the substitution $f'(\pm E) \to -\delta(\mu \mp E)$, and we obtain

$$\int_{-\infty}^{\infty} \chi_{\rm OZ} d\mu = 0. \qquad (50)$$

This sum rule is confirmed numerically with the three cases that we have examined. This relation suggests that $\chi_{\rm OZ}$ at $\mu = 0$ and that at the van Hove singularities are opposite, and they cancel each other.

B. Scaling of the diamagnetic peak at $\mu = 0$

In this subsection, we discuss the jumps in the orbital magnetic susceptibility, i.e., $\chi_{\rm LP} + \chi_1$, at the both ends of the gap (see Fig. 4). (Note that χ_2 does not contribute to jump.) We denote the magnitude of the jump as $\Delta\chi_{\rm dia}$. We expect that $\Delta\chi_{\rm dia}$ should be equal to the jump $3\pi t \chi_0/|m_0|$ obtained analytically in the effective Hamiltonian with two valleys considered [see Eq. (48)]. This scaling is explained by the effective "Landau diamagnetism" and "Pauli paramagnetism" in a Dirac electron system under a magnetic field, which is inversely proportional to effective mass m_0 [50]. The open circles in Fig. 5 show $\Delta\chi_{\rm dia}$ obtained from our numerical result for several values of t/Δ_0 at $t_2/t = 0.1$ and $k_B T/t = 0.001$. We can see that the open circles are excellently on the line $-3\pi t \chi_0/\Delta_0$. (Note that $|m_0| = \Delta_0$ at $t_2 = 0$.)

For finite t_2 cases, there are two different gaps at K and K′ points, the sizes of which we denote as $\Delta^{\rm K}$ and $\Delta^{\rm K'}$, respectively. Similarly, we find the jumps in the orbital magnetic susceptibility $\chi_{\rm LP} + \chi_1$ at the both ends of each gap, and each jump coincides with the calculated value for the corresponding gap, $\chi_{\rm 2DDirac}(\mu = 0, T, \Delta^{\rm K})$ or $\chi_{\rm 2DDirac}(\mu = 0, T, \Delta^{\rm K'})$.

C. Relation between $\chi_{\rm OZ}$ and the topological phase

We discuss the Berry curvature-related contribution $\chi_{\rm OZ}$ on the basis of the discussion previously given by the authors [21]. We concentrate on the case of $T = 0$ and $\mu = 0$, where the chemical potential is located in the gap. In this case, $\chi_{\rm OZ}$ is given by

$$\chi_{\rm OZ}(\mu = 0) = \frac{2e\mu_{\rm B}}{\hbar} \sum_{l:\rm occupied} \sum_{k,\sigma} \sigma \Omega_{l\sigma}^z. \qquad (51)$$

Note that the topology of wave functions in a spin-conserved system is characterized by the Chern number, $\mathrm{Ch}_{l,\sigma}$, where l and σ represent the band index and spin, respectively. The
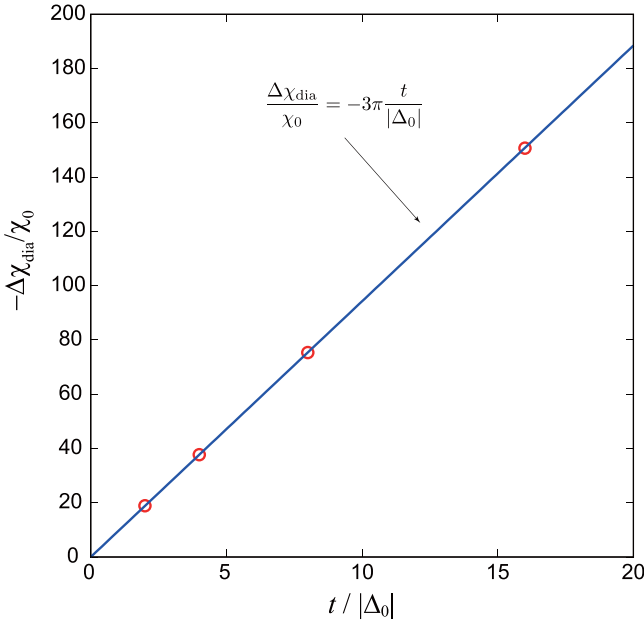
FIG. 5. Difference in magnetic susceptibility at the both ends of the gap in $\chi_1 + \chi_{LP}$, $\Delta\chi_{dia}$, as a function of t/Δ_0 at $t_2 = 0$ and $k_BT/t = 0.001$. Open circles: $\Delta\chi_{dia}$ obtained from our numerical result with $t/|\Delta_0| = 2.0, 4.0, 8.0,$ and 16.0. Solid line: Result obtained by the continuum model Eq. (48).

Chern number is explicitly given by

$$\text{Ch}_{l,\sigma} = \frac{1}{2\pi}\int d\boldsymbol{k}\,\Omega_{l\sigma} = \frac{2\pi}{L^2}\sum_{\boldsymbol{k}}\Omega_{l\sigma}, \qquad (52)$$

and takes an integer value. Using this relation, χ_{OZ} at $\mu = 0$ is given by

$$\chi_{OZ}(\mu = 0) = -\frac{4|e|\mu_B L^2}{h}\cdot\frac{1}{2}(\text{Ch}_{occ,\uparrow} - \text{Ch}_{occ,\downarrow}). \quad (53)$$

The right-hand side is proportional to the spin Chern number for the occupied band, a topological invariant for 2D TIs, defined by $(\text{Ch}_{occ,\uparrow} - \text{Ch}_{occ,\downarrow})/2$. This result indicates that $\chi_{OZ}(\mu = 0)$ is quantized in units of the universal value, $\chi_u = 4|e|\mu_B/h = 13.37\chi_0$ per area, reflecting the topological phase of materials.

Figure 6 shows the distribution of $\Omega_{l\sigma}(\boldsymbol{k})$ for some choices of parameters. Due to time-reversal symmetry, we have $\Omega_{l\uparrow}(-\boldsymbol{k}) = -\Omega_{l\downarrow}(\boldsymbol{k})$. For the case $t_2 = 0$ with different sizes of gaps [Figs. 6(a) and 6(b)], we can choose the eigenfunctions as $u_{l\uparrow\boldsymbol{k}}(\boldsymbol{r}) = u_{l\downarrow\boldsymbol{k}}(\boldsymbol{r})$. Therefore, the relation of the Berry curvature $\Omega_{l\sigma}(-\boldsymbol{k}) = -\Omega_{l\sigma}(\boldsymbol{k})$ holds and the summation of $\Omega_{l\sigma}$ in the Brillouin zone vanishes. For nonzero t_2, the relation $\Omega_{l\sigma}(-\boldsymbol{k}) = -\Omega_{l\sigma}(\boldsymbol{k})$ does not hold in general. Nevertheless, as long as $|\Delta_0| > 3\sqrt{3}|t_2|$ holds, the summation of the Berry curvature in the Brillouin zone is zero and $\chi_{OZ}(\mu = 0)$ also vanishes [Fig. 6(c)]. This corresponds to the fact that the system is still topologically trivial. However, for $|\Delta_0| < 3\sqrt{3}|t_2|$, the summation becomes nonzero [Fig. 6(d)]. In this parameter region, the system is topologically nontrivial and χ_{OZ} has a finite contribution. These results show that $\chi_{OZ}(\mu = 0)$ reflects the topological order of the Kane-Mele model. As the
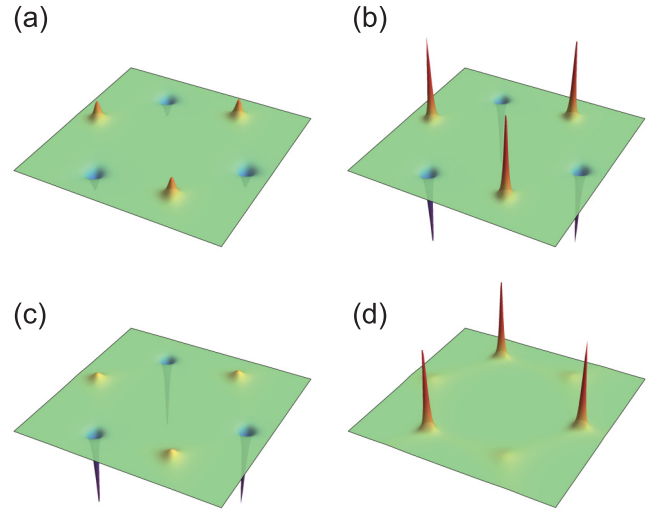

FIG. 6. The distribution of Berry curvature for the lower band with spin up at each parameter: (a) $\Delta_0/t = 1/4, t_2/t = 0$, (b) $\Delta_0/t = 1/8, t_2/t = 0$, (c) $\Delta_0/t = 1/4, t_2/t = \sqrt{3}/72$, and (d) $\Delta_0/t = 1/4, t_2/t = \sqrt{3}/24$. The integral of the Berry curvature over the whole Brillouin zone is zero when (a)–(c), while the counterpart of (d) is 2π. The state is topologically nontrivial only in the case of (d).

ratio of t_2 to Δ_0 changes, a jump in $\chi_{OZ}(\mu = 0)$ occurs at the topological phase transition.

Let us discuss experimental detection of the jump. For $\mu = 0$, the major contribution is χ_1 as well as χ_{OZ}. As shown in Sec. IV B, χ_1 diverges at the critical point $|\Delta_0| = 3\sqrt{3}|t_2|$. Although it seems difficult to detect the jump due to this divergence, χ_{OZ} will be experimentally observed according to the discussion below.

It is naturally assumed that the diverging interband contribution comes from the vicinities of K and K' points. As we mentioned, we can evaluate the contribution from K and K' at $\mu = 0$ as $\chi_{2DDirac}(\mu = 0, T, \Delta^K) + \chi_{2DDirac}(\mu = 0, T, \Delta^{K'})$. If we subtract this value from the observed total magnetic susceptibility, then we obtain the residue containing the jump in χ_{OZ}, i.e., the topological phase transition-related jump. Figure 7 shows the residue obtained by the above subtraction as a function of Δ_0/t. In this way, we can find the evidence of a topological phase transition. Note that the staggered on-site potential is variable by an electric field applied perpendicularly to the 2D plane. Therefore, the magnitude of the electric field corresponds to the horizontal axis in Fig. 7.

Figure 7 indicates that the magnitude of the jump in the total contribution slightly deviates from the predicted value $13.37\chi_0$. This deviation originates from the Berry-curvature-related term in the *purely* orbital, Berry-curvature-related contribution contained in χ_{occ2} [see Eqs. (29) and (30)], which also changes discontinuously at topological phase transitions. This fact does not contradict the statement that χ_{OZ} is universally quantized.

Note that the effect of the Berry curvature on the orbital magnetism was studied in some literatures [51–57]. In our formulation, the effect of the Berry curvature is included in χ_1, and causes the deviation of the jump from quantized value. However, this effect is purely orbital and does not affect χ_{OZ}.
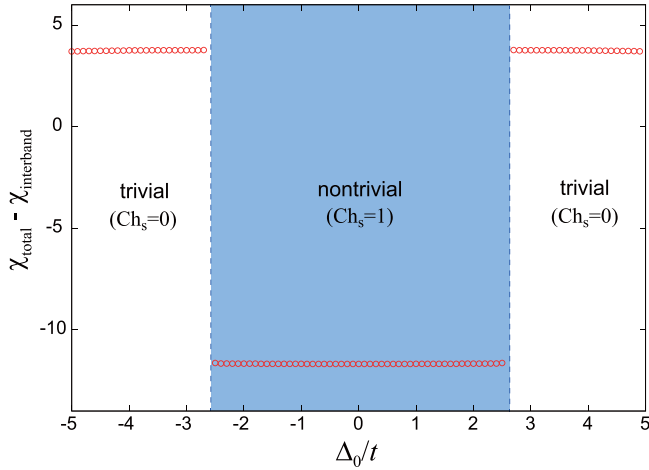
FIG. 7. Magnetic susceptibility with the interband contribution subtracted, where we define $\chi_{\text{interband}} = \chi_{\text{2DDirac}}(\mu = 0, T, \Delta^{\text{K}}) + \chi_{\text{2DDirac}}(\mu = 0, T, \Delta^{\text{K}'})$. The parameters t_2 and T are set to $t_2 = 0.1t$ and $k_B T = 0.001t$. The magnitude of jump mainly comes from the universal quantized value $\chi_u = 13.37\chi_0$; however, there exist an additional discontinuous contribution originating from a *purely* orbital term contained in χ_{occ2} in Eqs. (29) and (30). The overall positive shift originates from the plateau shown in Fig. 3.

V. DISCUSSIONS AND SUMMARY

Our present formulation focuses on the two-band model consisting of $2p_z$ orbitals. However, this method can be easily extended to other orbitals. In this case, the estimation of the hopping integrals and the effect of SOI should be modified. Nevertheless, the basic idea to obtain the hopping integrals and SOI-dependent integrals are the same as the idea developed in Appendix A. Note that, in our formulation, we can treat any crystal field using the original form of the spin-orbit interaction derived from the Dirac equation [the fourth term in Eq. (3)].

We enumerate some possible applications of the present method. First, our formulation will be applicable to the recently found candidate material WTe_2 [58–60], consisting of p and d orbitals. Since these orbitals have nonzero angular momentum, the matrix elements of the orbital magnetic moment Eq. (30) will be slightly modified.

The second example is silicene. In the present paper, as the first approximation, we have only considered the p_z orbitals. However, the effect of buckling may give some other interesting effects such as a mixing of the orbitals other than p_z orbital. In this case we need to treat six bands. Although fully analytic calculations for three or more band system will not be easy, it will be possible to evaluate each contribution by the combination of the present analytic method and some computational techniques.

In the present study, we assumed the spin conserving next-nearest-neighbor hopping, which is justified in the 2D systems as shown in Appendix A. It is very interesting to study the magnetic susceptibility especially the OZ cross term in the case where the spin is not conserved (for example Rashba term) both in the theoretical and experimental aspects. It remains a future problem.

In summary, we calculated the orbital, spin-Zeeman, and OZ magnetic susceptibility for the Kane-Mele model, using the formula written in terms of explicit wave functions, which enables us to evaluate each contribution taking account of the integration over the whole Brillouin zone and the summation over all the bands. The result includes additional contributions to the previous results [21], such as core electron diamagnetism, originating from the deformation of the wave functions by an external field. The numerical calculation has revealed some properties.

(i) It has been proved that the effect beyond the tight-binding and effective-model formulations does not change or affect the quantization of the OZ cross term. We have also found that if we can evaluate the size of the gap with some methods, we will be able to detect the OZ cross term experimentally and observe the change in the spin Chern number directly.

(ii) The OZ cross term can be a relatively large contribution, especially for insulating states and at the van Hove singularity, and is one of the major contributions to the magentic susceptibility.

(iii) The present analytic and numerical calculations show that χ_{OZ}, as well as the orbital contributions, satisfies the sum rule with respect to the chemical potential, $\int \chi_{\text{OZ}} d\mu = 0$.

We expect that the present method will serve as a useful tool for a profound understanding of orbital, Pauli, and orbital-Zeeman cross magnetic response of topological materials.

APPENDIX A: HOPPING INTEGRALS DUE TO THE SPIN-ORBIT INTERACTION

In this Appendix, we obtain hopping integrals due to the spin orbit interaction using LCAO in Eqs. (8) and (9). The matrix elements of SOI in Eq. (3) between $\varphi_{A\mathbf{k}}(\mathbf{r})$ and $\varphi_{B\mathbf{k}}(\mathbf{r})$ is given by

$$
\begin{aligned}
h_{\text{AB}\sigma\sigma'}^{\text{SO}}(\mathbf{k}) \simeq &\frac{1}{N} \sum_{\mathbf{R}_{Ai}, \mathbf{R}_{Bj}} e^{-i\mathbf{k}(\mathbf{R}_{Ai} - \mathbf{R}_{Bj})} \int d\mathbf{r} \Phi_\sigma^*(\mathbf{r} - \mathbf{R}_{Ai}) \frac{\hbar^2}{4m^2 c^2} \\
&\times (\boldsymbol{\sigma})_{\sigma\sigma'} \cdot \nabla \{V_A(\mathbf{r} - \mathbf{R}_{Ai}) + V_B(\mathbf{r} - \mathbf{R}_{Bj})\} \\
&\times \{-i\nabla \Phi_{\sigma'}(\mathbf{r} - \mathbf{R}_{Bj})\},
\end{aligned}
\tag{A1}
$$

where we have chosen $V_A(\mathbf{r} - \mathbf{R}_{Ai}) + V_B(\mathbf{r} - \mathbf{R}_{Bj})$ out of $V(\mathbf{r})$ since the other terms in $V(\mathbf{r})$ should be small at $\mathbf{r} = \mathbf{R}_{Ai}$ or $\mathbf{r} = \mathbf{R}_{Bj}$. We show the spin component of the wave functions explicitly. Other matrix elements $h_{AA\sigma\sigma'}^{\text{SO}}(\mathbf{k})$ and $h_{BB\sigma\sigma'}^{\text{SO}}(\mathbf{k})$ are expressed in similar ways, which are to be discussed later.

The dominant contribution in Eq. (A1) is between the nearest-neighbor-sites. By choosing an appropriate
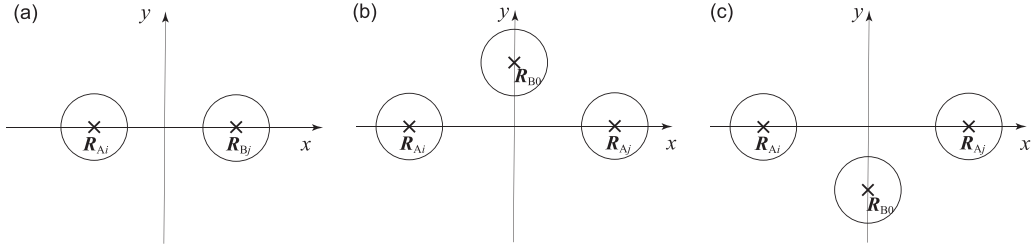
FIG. 8. Configurations of atoms for (a) nearest-neighbor and (b), (c) next-nearest-neighbor hoppings.

coordinates, the r integral can be expressed as in Fig. 8(a). We can assume that $V_A(r - R_{Ai})$, $V_B(r - R_{Bj})$, $\Phi_\sigma(r - R_{Ai})$ and $\Phi_{\sigma'}(r - R_{Bj})$ are even functions with respect to y. Therefore, when one of the two nablas in Eq. (A1) is $\frac{\partial}{\partial y}$, the r integral vanishes. We can also assume that $V_A(r - R_{Ai})$ and $V_B(r - R_{Bj})$ are even functions with respect to z, while $\Phi_\sigma(r - R_{Ai})$ and $\Phi_{\sigma'}(r - R_{Bj})$ are odd functions. Therefore, when one of the two nablas in Eq. (A1) is $\frac{\partial}{\partial z}$, the r integral vanishes again. As a result, $h^{SO}_{AB\sigma\sigma'}(k)$ vanishes.

Next, we discuss $h^{SO}_{AA\sigma\sigma'}(k)$. The dominant contribution is between the next-nearest-neighbor pair,

$$
h^{SO}_{AA\sigma\sigma'}(k) \simeq \frac{1}{N} \sum_{R_{Ai},R_{Aj}} e^{-ik(R_{Ai}-R_{Aj})} \int dr \Phi_\sigma^*(r - R_{Ai}) \frac{\hbar^2}{4m^2c^2}
$$
$$
\times (\sigma)_{\sigma\sigma'} \cdot \nabla \{V_A(r - R_{Ai}) + V_B(r - R_{B0})
$$
$$
+ V_A(r - R_{Aj})\} \times \{-i\nabla \Phi_{\sigma'}(r - R_{Aj})\}. \quad \text{(A2)}
$$

The appropriate coordinates give the configurations as in Figs. 8(b) and 8(c). In the following, we neglect the overlap integral s in $\Phi_\sigma(r)$ and replace $\Phi_\sigma(r)$ with $\phi_\sigma(r)$. All the potentials in Eq. (A2) will be even functions with respect to z, while $\phi_\sigma^*(r - R_{Ai})$ and $\phi_{\sigma'}(r - R_{Aj})$ are odd functions. Therefore, as in the case of Eq. (A1), when one of the two nablas is $\frac{\partial}{\partial z}$, the r integral vanishes. Similarly, the terms in Eq. (A2) with $V_A(r - R_{Ai})$ and $V_A(r - R_{Aj})$ are even functions with respect to y. Therefore, they vanish as in the case of Eq. (A1). In contrast, the term with $V_B(r - R_{B0})$ gives a nonzero value,

$$
\frac{\hbar^2}{4m^2c^2} \int dr \phi_\sigma^*(r - R_{Ai})(\sigma^z)_{\sigma\sigma'} \left[\frac{\partial}{\partial x} V_B(r - R_{B0}) \right.
$$
$$
\times \left(-i\frac{\partial}{\partial y} \right) \phi_{\sigma'}(r - R_{Aj}) - \frac{\partial}{\partial y} V_B(r - R_{B0})
$$
$$
\left. \times \left(-i\frac{\partial}{\partial x} \right) \phi_{\sigma'}(r - R_{Aj}) \right] dr. \quad \text{(A3)}
$$

If we assume $R_{B0} = (0, b, 0)$, $R_{Aj} = (a, 0, 0)$, $V_B(r - R_{B0}) = V_B(\rho, z)$, and $\phi_{\sigma'}(r - R_{Aj}) = \phi_{\sigma'}(\rho_A, z)$ with $\rho = \sqrt{x^2 + (y - b)^2}$ and $\rho_A = \sqrt{(x - a)^2 + y^2}$ for Fig. 8(b), then the integral in Eq. (A3) becomes

$$
-i \int dr \phi_\sigma^*(r - R_{Ai})(\sigma^z)_{\sigma\sigma'}(ay + bx - ab)\frac{1}{\rho \rho_A}
$$
$$
\times \frac{\partial V_B(\rho, z)}{\partial \rho} \frac{\partial \phi_{\sigma'}(\rho_A, z)}{\partial \rho_A}. \quad \text{(A4)}
$$

Similarly, for Fig. 8(c), we obtain

$$
-i \int dr \phi_\sigma^*(r - R_{Ai})(\sigma^z)_{\sigma\sigma'}(ay - bx + ab)\frac{1}{\rho' \rho_A}
$$
$$
\times \frac{\partial V_B(\rho', z)}{\partial \rho'} \frac{\partial \phi_{\sigma'}(\rho_A, z)}{\partial \rho_A}, \quad \text{(A5)}
$$

with $\rho' = \sqrt{x^2 + (y + b)^2}$. When we make the change of the integral variable $y \to -y$, we can see that Eq. (A5) exactly equals (-1) times Eq. (A4). In the same way, we can obtain $h^{SO}_{BB\sigma\sigma'}(k)$. These next-nearest-neighbor hoppings exactly have the same symmetry as Kane-Mele assumed, although the absolute value and the sign is determined from the details of the functional forms in Eq. (A3).

The present derivation can be applied to the antisymmetric SOI due to the local inversion symmetry breaking [61,62]. In transition metal dichalcogenides, such as WTe$_2$, the inversion symmetry breaks locally due to odd-parity crystal field. This symmetry breaking gives rise to local hybridization of wave functions of different parities. The combination of this hybridization and $L \cdot s$ coupling generates antisymmetric SOI such as the Rashba-type SOI. In our formulation, we can treat any crystal field, and the hybridization of wave functions of different parities are naturally included. Also, the fourth term in Eq. (3) is the original form of spin-orbit interaction derived from the Dirac equation, and it is exactly the $L \cdot s$ coupling when we consider a single-atom potential. Therefore, our formulation properly describe the antisymmetric SOI due to the local symmetry breaking.

APPENDIX B: INTEGRATION FORMULAS

Table II shows the order estimates of several quantities with respect to the "overlap integrals" s, t, or t_2 (all denoted as s in the following) for the two cases of $\Delta_0 \gg t$ and $\Delta_0 \lesssim t$. Note that $E_{k\sigma} = \sqrt{\Delta_{k\sigma}^2 + \varepsilon_k^2}$. In the following calculations, we keep the terms up to the order of s^1.

First, we show several integration formulas using $u_{k\sigma}^\pm(r)$ of Eqs. (19) and (20), which will be used in calculating χ. To simplify the expressions, we abbreviate ε_k, θ_k, $E_{k\sigma}$, $\Delta_{k\sigma}$, and $\eta_{k\sigma}$ as ε, θ, E, Δ, and η, respectively, in the following Appendices. Furthermore, we use the abbreviations

$$
\varepsilon_\mu = \frac{\partial \varepsilon}{\partial k_\mu}, \quad \theta_\mu = \frac{\partial \theta}{\partial k_\mu}, \quad E_\mu = \frac{\partial E}{\partial k_\mu}, \quad \Delta_\mu = \frac{\partial \Delta}{\partial k_\mu},
$$
$$
\eta_\mu = \frac{\partial \eta}{\partial k_\mu}, \quad \text{(B1)}
$$

TABLE II. Order estimations of several quantities with respect to the "overlap integral" s, t, or t_2 (all denoted as s). Here μ is x or y, and $\eta_{k\sigma}$ and θ_k are defined in Eqs. (21)–(23).

	$\Delta_0 \gg t$	$\Delta_0 \lesssim t$
$E_{k\sigma}$	1	s
$\frac{\partial E_{k\sigma}}{\partial k_\mu}$	s	s
$\eta_{k\sigma}$	1	1
$\frac{\partial \eta_{k\sigma}}{\partial k_\mu}$	s	1
θ_k	1	1
$\frac{\partial \theta_k}{\partial k_\mu}$	1	1
$\Delta_{k\sigma}$	1	s
$\frac{\partial \Delta_{k\sigma}}{\partial k_\mu}$	s	s

$$\varepsilon_{\mu\nu} = \frac{\partial^2 \varepsilon}{\partial k_\mu \partial k_\nu}, \quad \theta_{\mu\nu} = \frac{\partial^2 \theta}{\partial k_\mu \partial k_\nu}, \quad E_{\mu\nu} = \frac{\partial^2 E}{\partial k_\mu \partial k_\nu},$$

$$\Delta_{\mu\nu} = \frac{\partial^2 \Delta}{\partial k_\mu \partial k_\nu}, \quad \eta_{\mu\nu} = \frac{\partial^2 \eta}{\partial k_\mu \partial k_\nu}, \tag{B2}$$

for μ, $\nu = x$ or y. Then we obtain

$$\text{(F1)} \int u_{k\sigma}^{\pm *} \frac{\partial u_{k\sigma}^{\pm}}{\partial k_\mu} d\mathbf{r} = \pm i \frac{\Delta}{2E} \theta_\mu + O(s^2),$$

$$\text{(F2)} \int u_{k\sigma}^{\pm *} \frac{\partial u_{k\sigma}^{\mp}}{\partial k_\mu} d\mathbf{r} = i \frac{\varepsilon}{2E} \theta_\mu \pm \eta_\mu + O(s^2),$$

$$\text{(F3)} \int \frac{\partial u_{k\sigma}^{\pm *}}{\partial k_\mu} \frac{\partial u_{k\sigma}^{\pm}}{\partial k_\nu} d\mathbf{r} = \langle x_\mu x_\nu \rangle + \frac{1}{4} \theta_\mu \theta_\nu + \eta_\mu \eta_\nu$$
$$\pm i \frac{\varepsilon}{2E} (\theta_\mu \eta_\nu - \theta_\nu \eta_\mu) \mp \frac{\varepsilon}{E} \text{Re} X_{\mu\nu} + O(s^2),$$

$$\text{(F4)} \int \frac{\partial u_{k\sigma}^{\pm *}}{\partial k_\mu} \frac{\partial u_{k\sigma}^{\mp}}{\partial k_\nu} d\mathbf{r} = -i \frac{\Delta}{2E} (\theta_\mu \eta_\nu - \theta_\nu \eta_\mu) + Y_{\mu\nu}^{\pm} + O(s^2),$$

$$\text{(F5)} \int u_{k\sigma}^{\pm *} \frac{\partial H_k}{\partial k_\mu} u_{k\sigma}^{\pm} d\mathbf{r} = \pm E_\mu,$$

$$\text{(F6)} \int u_{k\sigma}^{\pm *} \frac{\partial H_k}{\partial k_\mu} u_{k\sigma}^{\mp} d\mathbf{r} = \mp 2E \int u_{k\sigma}^{\pm *} \frac{\partial u_{k\sigma}^{\mp}}{\partial k_\mu} d\mathbf{r} = \mp i \varepsilon \theta_\mu$$
$$- 2E\eta_\mu + O(s^2),$$

$$\text{(F7)} \int u_{k\sigma}^{\pm *} \frac{\partial H_k}{\partial k_\mu} \frac{\partial u_{k\sigma}^{\pm}}{\partial k_\nu} d\mathbf{r} = -\frac{\hbar^2}{2m} \delta_{\mu\nu} \pm \frac{1}{2} E_{\mu\nu} + i \frac{\Delta}{2E} E_\mu \theta_\nu$$
$$- i\varepsilon(\eta_\mu \theta_\nu - \eta_\nu \theta_\mu) + O(s^2),$$

$$\text{(F8)} \int u_{k\sigma}^{\mp *} \frac{\partial H_k}{\partial k_\mu} \frac{\partial u_{k\sigma}^{\pm}}{\partial k_\nu} d\mathbf{r} = \pm \frac{i}{2} \varepsilon_\nu \theta_\mu - \eta_\mu E_\nu - E\eta_{\mu\nu}$$
$$\mp E Y_{\mu\nu}^{\mp} \pm \frac{i}{2} \varepsilon \theta_{\mu\nu} + O(s^2), \tag{B3}$$

with

$$X_{\mu\nu} = \sum_{\mathbf{R}} e^{-i\theta_k} e^{-i\mathbf{k}\cdot\mathbf{R}} \langle x_\mu x_\nu \rangle_{\mathbf{R}},$$

$$Y_{\mu\nu}^{\pm} = \frac{\Delta}{E} \text{Re} X_{\mu\nu} \pm i \text{Im} X_{\mu\nu}. \tag{B4}$$

The meaning of the $\mathbf{R}$ summation and $\langle \cdots \rangle_{\mathbf{R}}$ are shown below. $X_{\mu\nu}$ and $Y_{\mu\nu}^{\pm}$ are in the order of s.

1. Derivation of (F1)–(F4)

The k_μ derivative of $u_{k\sigma}^{+}$ becomes

$$\frac{\partial u_{k\sigma}^{+}}{\partial k_\mu} = \frac{i}{2} \theta_\mu \cos 2\eta u_{k\sigma}^{+} + \left(\frac{i}{2} \theta_\mu \sin 2\eta - \eta_\mu \right) u_{k\sigma}^{-} + e^{\frac{i}{2}\theta} \cos \eta \frac{\partial \varphi_{Ak}}{\partial k_\mu} - e^{-\frac{i}{2}\theta} \sin \eta \frac{\partial \varphi_{Bk}}{\partial k_\mu}. \tag{B5}$$

To obtain (F1), we must calculate the integral of product of Bloch wave function $u_{k\sigma}^{\pm}$ and k-derivative of $\varphi_{A/Bk}(\mathbf{r})$. They become

$$\int u_{k\sigma}^{+*} \frac{\partial \varphi_{Ak}}{\partial k_\mu} d\mathbf{r} = - e^{-\frac{i}{2}\theta} \cos \eta \frac{i}{N} \sum_{\mathbf{R}_{Ai}, \mathbf{R}_{Aj}} e^{-i\mathbf{k}(\mathbf{R}_{Ai}-\mathbf{R}_{Aj})} \int (x - R_{Ajx}) \Phi^*(\mathbf{r} - \mathbf{R}_{Ai}) \Phi(\mathbf{r} - \mathbf{R}_{Aj}) d\mathbf{r}$$
$$+ e^{\frac{i}{2}\theta} \sin \eta \frac{i}{N} \sum_{\mathbf{R}_{Aj}, \mathbf{R}_{Bi}} e^{i\mathbf{k}(\mathbf{R}_{Aj}-\mathbf{R}_{Bi})} \int (x - R_{Ajx}) \Phi^*(\mathbf{r} - \mathbf{R}_{Bi}) \Phi(\mathbf{r} - \mathbf{R}_{Aj}) d\mathbf{r}. \tag{B6}$$

Hereafter, we only consider the on-site and adjacent-site contributions. Then we obtain

$$\int u_{k\sigma}^{+*} \frac{\partial \varphi_{Ak}}{\partial k_\mu} d\mathbf{r} = - e^{-\frac{i}{2}\theta} \cos \eta \frac{i}{N} \sum_{\mathbf{R}_{Ai}} \int (x - R_{Aix}) \Phi^*(\mathbf{r} - \mathbf{R}_{Ai}) \Phi(\mathbf{r} - \mathbf{R}_{Ai}) d\mathbf{r}$$
$$+ e^{\frac{i}{2}\theta} \sin \eta \frac{i}{N} \sum_{\substack{\mathbf{R}_{Aj}, \mathbf{R}_{Bi} \\ \mathbf{R}_{Aj}-\mathbf{R}_{Bi}=n.n.}} e^{i\mathbf{k}(\mathbf{R}_{Aj}-\mathbf{R}_{Bi})} \int (x - R_{Ajx}) \Phi^*(\mathbf{r} - \mathbf{R}_{Bi}) \Phi(\mathbf{r} - \mathbf{R}_{Aj}) d\mathbf{r}$$
$$= - i e^{-\frac{i}{2}\theta} \cos \eta \langle x \rangle + i \sin \eta \sum_{\mathbf{R}} e^{i\mathbf{k}\mathbf{R}} \langle x \rangle_{(-\mathbf{R})}, \tag{B7}$$

where $\boldsymbol{R}$ runs over the three vectors from a B site to its adjacent A sites. The expectation values $\langle O \rangle$ and $\langle O \rangle_{\boldsymbol{R}}$ are defined as [23,24]

$$\langle O \rangle = \int \Phi^*(\boldsymbol{r}) \hat{O} \Phi(\boldsymbol{r}) d\boldsymbol{r} \tag{B8}$$

and

$$\langle O \rangle_{\boldsymbol{R}} = \int d\boldsymbol{r} \Phi^*(\boldsymbol{r} - \boldsymbol{R}) \hat{O} \Phi(\boldsymbol{r}) d\boldsymbol{r}. \tag{B9}$$

We can see that $\langle x \rangle$ and $\langle x \rangle_{\boldsymbol{R}}$ are in the order of s^2. Therefore, we obtain

$$\int u_{\boldsymbol{k}\sigma}^{+*} \frac{\partial \varphi_{A\boldsymbol{k}}}{\partial k_\mu} d\boldsymbol{r} = O(s^2). \tag{B10}$$

For $\partial \varphi_{B\boldsymbol{k}} / \partial k_\mu$, we have the similar relation

$$\int u_{\boldsymbol{k}\sigma}^{+*} \frac{\partial \varphi_{B\boldsymbol{k}}}{\partial k_\mu} d\boldsymbol{r} = O(s^2). \tag{B11}$$

Using Eqs. (B10) and (B11), we have

$$\int u_{\boldsymbol{k}\sigma}^{+*} \frac{\partial u_{\boldsymbol{k}\sigma}^+}{\partial k_\mu} d\boldsymbol{r} = \frac{i}{2} \theta_\mu \cos 2\eta + O(s^2) \tag{B12}$$

and

$$\int u_{\boldsymbol{k}\sigma}^{+*} \frac{\partial u_{\boldsymbol{k}\sigma}^-}{\partial k_\mu} d\boldsymbol{r} = \frac{i}{2} \theta_\mu \sin 2\eta + \eta_\mu + O(s^2). \tag{B13}$$

If we substitute $\eta \to \eta - \pi/2$, then $u_{\boldsymbol{k}\sigma}^+$ and $u_{\boldsymbol{k}\sigma}^-$ become $u_{\boldsymbol{k}\sigma}^-$ and $-u_{\boldsymbol{k}\sigma}^+$, respectively. With the relations

$$\sin 2\eta = \frac{\varepsilon}{E}, \quad \cos 2\eta = \frac{\Delta}{E}, \tag{B14}$$

we obtain (F1) and (F2).

Similar to the derivation of (F1) and (F2), we obtain

$$\int \frac{\partial \varphi_{A\boldsymbol{k}}^*}{\partial k_\mu} \frac{\partial \varphi_{A\boldsymbol{k}}}{\partial k_\nu} d\boldsymbol{r} = \int \frac{\partial \varphi_{B\boldsymbol{k}}^*}{\partial k_\mu} \frac{\partial \varphi_{B\boldsymbol{k}}}{\partial k_\nu} d\boldsymbol{r} = \langle x_\mu x_\nu \rangle + O(s^2) \tag{B15}$$

and

$$\int \frac{\partial \varphi_{A\boldsymbol{k}}^*}{\partial k_\mu} \frac{\partial \varphi_{B\boldsymbol{k}}}{\partial k_\nu} d\boldsymbol{r} = \sum_{\boldsymbol{R}} e^{-i\boldsymbol{k}\cdot\boldsymbol{R}} \langle x_\mu x_\nu \rangle_{\boldsymbol{R}} + O(s^2). \tag{B16}$$

Using these relations and substitution of $\eta \to \eta - \pi/2$, we obtain (F3) and (F4). In the different sign cases (e.g., $\int \frac{\partial u_{\boldsymbol{k}\sigma}^{+*}}{\partial k_\mu} \frac{\partial u_{\boldsymbol{k}\sigma}^-}{\partial k_\nu} d\boldsymbol{r}$), we can calculate the integral in almost the same way.

2. Derivation of (F5) and (F6)

We start from the Schrödinger equation,

$$H_{\boldsymbol{k}} u_{\boldsymbol{k}\sigma}^\pm = \pm E u_{\boldsymbol{k}\sigma}^\pm. \tag{B17}$$

Differentiating the both sides of this equation by k_μ, we obtain

$$\left(\frac{\partial H_{\boldsymbol{k}}}{\partial k_\mu} \mp \frac{\partial E}{\partial k_\mu} \right) u_{\boldsymbol{k}\sigma}^\pm = (\pm E - H_{\boldsymbol{k}}) \frac{\partial u_{\boldsymbol{k}\sigma}^\pm}{\partial k_\mu}. \tag{B18}$$

When we multiply $u_{\boldsymbol{k}\sigma}^{\pm*}$ and integrate the product, we obtain (F5). Similarly, multiplying $u_{\boldsymbol{k}\sigma}^{\mp*}$ and using (F2), we obtain (F6).

3. Derivation of (F7)

To obtain (F7), we first calculate

$$\int u_{\boldsymbol{k}\sigma}^{\pm*} \left(\frac{\partial H_{\boldsymbol{k}}}{\partial k_\mu} \frac{\partial u_{\boldsymbol{k}\sigma}^\pm}{\partial k_\nu} + \frac{\partial H_{\boldsymbol{k}}}{\partial k_\nu} \frac{\partial u_{\boldsymbol{k}\sigma}^\pm}{\partial k_\mu} \right) d\boldsymbol{r} \tag{B19}$$

and

$$\int u_{\boldsymbol{k}\sigma}^{\pm*} \left(\frac{\partial H_{\boldsymbol{k}}}{\partial k_\mu} \frac{\partial u_{\boldsymbol{k}\sigma}^\pm}{\partial k_\nu} - \frac{\partial H_{\boldsymbol{k}}}{\partial k_\nu} \frac{\partial u_{\boldsymbol{k}\sigma}^\pm}{\partial k_\mu} \right) d\boldsymbol{r}. \tag{B20}$$

Differentiating the both sides of Eq. (B18) by k_ν, we obtain

$$\left(\frac{\hbar^2}{m} \delta_{\mu\nu} \mp \frac{\partial^2 E}{\partial k_\mu \partial k_\nu} \right) u_{\boldsymbol{k}\sigma}^\pm + \left(\frac{\partial H_{\boldsymbol{k}}}{\partial k_\mu} \mp \frac{\partial E}{\partial k_\mu} \right) \frac{\partial u_{\boldsymbol{k}\sigma}^\pm}{\partial k_\nu} + \left(\frac{\partial H_{\boldsymbol{k}}}{\partial k_\nu} \mp \frac{\partial E}{\partial k_\nu} \right) \frac{\partial u_{\boldsymbol{k}\sigma}^\pm}{\partial k_\mu} + (H_{\boldsymbol{k}} \mp E) \frac{\partial^2 u_{\boldsymbol{k}\sigma}^\pm}{\partial k_\mu \partial k_\nu} = 0. \tag{B21}$$

Here we have used the relation

$$\frac{\partial^2 H_{\boldsymbol{k}}}{\partial k_\mu \partial k_\nu} = \frac{\hbar^2}{m} \delta_{\mu\nu}. \tag{B22}$$

Then, multiplying $u_{\boldsymbol{k}\sigma}^{\pm*}$ and integrating, we obtain

$$\int u_{\boldsymbol{k}\sigma}^{\pm*} \left(\frac{\partial H_{\boldsymbol{k}}}{\partial k_\mu} \frac{\partial u_{\boldsymbol{k}\sigma}^\pm}{\partial k_\nu} + \frac{\partial H_{\boldsymbol{k}}}{\partial k_\nu} \frac{\partial u_{\boldsymbol{k}\sigma}^\pm}{\partial k_\mu} \right) d\boldsymbol{r} = -\frac{\hbar^2}{m} \delta_{\mu\nu} \pm E_{\mu\nu} + i\frac{\Delta}{2E} (E_\mu \theta_\nu + E_\nu \theta_\mu) + O(s^2). \tag{B23}$$

Here we have used the formula (F1).

Next, we calculate Eq. (B20). By using the explicit forms of $\frac{\partial H_{\boldsymbol{k}}}{\partial k_y}$ and $\frac{\partial u_{\boldsymbol{k}\sigma}^\pm}{\partial k_x}$ and using the fact that $\phi(\boldsymbol{r})$ (p_z orbital) is an eigenstate of angular momentum, $L_z \phi(\boldsymbol{r}) = 0$, we can write

$$\frac{\partial H_{\boldsymbol{k}}}{\partial k_y} \frac{\partial u_{\boldsymbol{k}\sigma}^\pm}{\partial k_x} - \frac{\partial H_{\boldsymbol{k}}}{\partial k_x} \frac{\partial u_{\boldsymbol{k}\sigma}^\pm}{\partial k_y} = \frac{\partial H_{\boldsymbol{k}}}{\partial k_y} \left[\pm \left(i\frac{\theta_x}{2} \frac{\Delta}{E} + \frac{s\varepsilon_x}{2t} \frac{\varepsilon}{E} \right) u_{\boldsymbol{k}\sigma}^\pm + \left(i\frac{\theta_x}{2} \frac{\varepsilon}{E} \mp \eta_x \pm \frac{is\varepsilon}{2t} \theta_x - \frac{s\varepsilon_x}{2t} \frac{\Delta}{E} \right) u_{\boldsymbol{k}\sigma}^\mp \right]$$
$$- (x \leftrightarrow y) + O(s^2). \tag{B24}$$

Then we multiply $u_{k\sigma}^{\pm*}$ and integrate the product. After some algebra, we obtain

$$\int u_{k\sigma}^{\pm*}\left(\frac{\partial H_k}{\partial k_\mu}\frac{\partial u_{k\sigma}^\pm}{\partial k_\nu} - \frac{\partial H_k}{\partial k_\nu}\frac{\partial u_{k\sigma}^\pm}{\partial k_\mu}\right)dr = i\frac{\Delta}{2E}(E_\mu\theta_\nu - E_\nu\theta_\mu) - 2i\varepsilon(\eta_\mu\theta_\nu - \eta_\nu\theta_\mu) + O(s^2). \tag{B25}$$

Here, we have used the formulas (F5), and (F6). Combining Eqs. (B23) and (B25), we obtain (F7).

4. Derivation of (F8)

Similar to the derivation of (F7), we calculate

$$\int u_{k\sigma}^{\mp*}\left(\frac{\partial H_k}{\partial k_\mu}\frac{\partial u_{k\sigma}^\pm}{\partial k_\mu} + \frac{\partial H_k}{\partial k_\nu}\frac{\partial u_{k\sigma}^\pm}{\partial k_\nu}\right)dr \tag{B26}$$

and

$$\int u_{k\sigma}^{\mp*}\left(\frac{\partial H_k}{\partial k_\mu}\frac{\partial u_{k\sigma}^\pm}{\partial k_\mu} - \frac{\partial H_k}{\partial k_\nu}\frac{\partial u_{k\sigma}^\pm}{\partial k_\nu}\right)dr. \tag{B27}$$

First, we multiply $u_{k\sigma}^{\mp*}$ to Eq. (B21) and integrate the product. Then we obtain

$$\int u_{k\sigma}^{\mp*}\left(\frac{\partial H_k}{\partial k_\mu}\frac{\partial u_{k\sigma}^\pm}{\partial k_\nu} + \frac{\partial H_k}{\partial k_\nu}\frac{\partial u_{k\sigma}^\pm}{\partial k_\mu}\right)dr = \pm E_\mu \int u_{k\sigma}^{\mp*}\frac{\partial u_{k\sigma}^\pm}{\partial k_\nu}dr \pm E_\nu \int u_{k\sigma}^{\mp*}\frac{\partial u_{k\sigma}^\pm}{\partial k_\mu}dr \pm 2E \int u_{k\sigma}^{\mp*}\frac{\partial^2 u_{k\sigma}^\pm}{\partial k_\mu \partial k_\nu}dr. \tag{B28}$$

To calculate the last term, by differentiating (F2) by k_ν, we find a relation,

$$\int u_{k\sigma}^{\pm*}\frac{\partial^2 u_{k\sigma}^\mp}{\partial k_\mu \partial k_\nu}dr = -\int \frac{\partial u_{k\sigma}^{\pm*}}{\partial k_\mu}\frac{\partial u_{k\sigma}^\mp}{\partial k_\nu}dr + \frac{\partial}{\partial k_\mu}\int u_{k\sigma}^{\pm*}\frac{\partial u_{k\sigma}^\mp}{\partial k_\nu}dr$$

$$= i\frac{\Delta}{2E}(\theta_\mu\eta_\nu + \theta_\nu\eta_\mu) + i\frac{\varepsilon}{2E}\theta_{\mu\nu} \pm \eta_{\mu\nu} - Y_{\mu\nu}^\pm + O(s^2), \tag{B29}$$

where we have used a relation Eq. (C1) or Eq. (C2). Substitution of this relation to Eq. (B28) leads to

$$\int u_{k\sigma}^{\mp*}\left(\frac{\partial H_k}{\partial k_\mu}\frac{\partial u_{k\sigma}^\pm}{\partial k_\nu} + \frac{\partial H_k}{\partial k_\nu}\frac{\partial u_{k\sigma}^\pm}{\partial k_\mu}\right)dr = \pm\frac{i}{2}(\varepsilon_\mu\theta_\nu + \varepsilon_\nu\theta_\mu) - (E_\mu\eta_\nu + E_\nu\eta_\mu) \pm i\varepsilon\theta_{\mu\nu} \mp 2EY_{\mu\nu}^\mp - 2E\eta_{\mu\nu} + O(s^2). \tag{B30}$$

However, using Eq. (B24), we obtain

$$\int u_{k\sigma}^{\mp*}\left(\frac{\partial H_k}{\partial k_\mu}\frac{\partial u_{k\sigma}^\pm}{\partial k_\nu} - \frac{\partial H_k}{\partial k_\nu}\frac{\partial u_{k\sigma}^\pm}{\partial k_\mu}\right)dr = \pm\left(i\frac{\Delta\theta_\nu}{2E} + \frac{s\varepsilon\varepsilon_\nu}{2tE}\right)\int u_{k\sigma}^{\mp*}\frac{\partial H_k}{\partial k_\mu}u_{k\sigma}^\pm dr - (\mu \leftrightarrow \nu) + \left(i\frac{\varepsilon\theta_\nu}{2E} \mp \eta_\nu \pm \frac{is\varepsilon}{2t}\theta_\nu - \frac{s\Delta\varepsilon_\nu}{2tE}\right)$$

$$\times \int u_{k\sigma}^{\mp*}\frac{\partial H_k}{\partial k_\mu}u_{k\sigma}^\mp dr - (\mu \leftrightarrow \nu) = \mp\frac{i}{2}(\varepsilon_\mu\theta_\nu - \varepsilon_\nu\theta_\mu) - \frac{1}{2E}(\varepsilon_\mu\Delta_\nu - \varepsilon_\nu\Delta_\mu) + O(s^2), \tag{B31}$$

where we have used (F5) and (F6). Combining Eqs. (B30) and (B31), we obtain (F8).

APPENDIX C: SEVERAL RELATIONS BETWEEN MOMENTUM DERIVATIVES

We find various relations between E_μ, η_μ, ε_μ, Δ_μ, and θ_μ, which are used in various occasions. Using $\sin 2\eta = \varepsilon/E$ and $\cos 2\eta = \Delta/E$, we can see

$$\frac{\partial}{\partial k_\mu}\left(\frac{\varepsilon}{E}\right) = \frac{\partial}{\partial k_\mu}\sin 2\eta = 2\eta_\mu \cos 2\eta = \frac{2\Delta}{E}\eta_\mu. \tag{C1}$$

By writing explicitly the left-hand side, we obtain

$$\Delta\eta_\mu + \frac{\varepsilon}{2E}E_\mu = \frac{\varepsilon_\mu}{2}. \tag{C2}$$

Similarly, from the derivative of $\Delta/E = \cos 2\eta$, we have

$$-\varepsilon\eta_\mu + \frac{\Delta}{2E}E_\mu = \frac{\Delta_\mu}{2}, \tag{C3}$$

which was used in the text Eq. (35). Furthermore, by making the k_ν derivative of Eqs. (C2) and (C3), we obtain

$$E\eta_{\mu\nu} + E_\mu\eta_\nu + E_\nu\eta_\mu = \frac{1}{2E}(\Delta\varepsilon_{\mu\nu} - \varepsilon\Delta_{\mu\nu}) \tag{C4}$$

and

$$E_{\mu\nu} - 4E\eta_\mu\eta_\nu = \frac{1}{E}(\varepsilon\varepsilon_{\mu\nu} + \Delta\Delta_{\mu\nu}). \tag{C5}$$

In the previous paper, we obtained the following relationships [24]:

$$\varepsilon(\theta_x^2 + \theta_y^2) - \varepsilon_{xx} - \varepsilon_{yy} = a^2\varepsilon, \ \varepsilon(\theta_{xx} + \theta_{yy}) + 2\varepsilon_x\theta_x + 2\varepsilon_y\theta_y = 0, \tag{C6}$$

with a being the length between the nearest-neighbor carbons. These special relations hold since ε and θ are closely related to each other through γ_k. Here we find additional relations.

Let us consider

$$\sum_R (R_x^2 - R_y^2)e^{-ik\cdot R}, \tag{C7}$$

where R runs over the three vectors from a B site to its adjacent A sites. By using the explicit three vectors in Fig. 1, we can see that it is equal to

$$-ia\frac{\partial}{\partial k_y}\sum_R e^{-ik\cdot R}. \tag{C8}$$

Then, from the definitions of γ_k and θ, we can obtain the relationship

$$\left(-\frac{\partial^2}{\partial k_x^2} + \frac{\partial^2}{\partial k_y^2}\right)|\gamma_k|e^{i\theta} = -ia\frac{\partial}{\partial k_y}|\gamma_k|e^{i\theta}. \tag{C9}$$

By taking the real and imaginary part of both sides, we obtain

$$\varepsilon(\theta_x^2 - \theta_y^2) - \varepsilon_{xx} + \varepsilon_{yy} = a\varepsilon\theta_y, \ \varepsilon(\theta_{xx} - \theta_{yy}) + 2\varepsilon_x\theta_x - 2\varepsilon_y\theta_y = a\varepsilon_y. \tag{C10}$$

From Eqs. (C6) and (C10), we can see

$$\varepsilon_{xx} = \varepsilon\theta_x^2 - \frac{a^2}{2}\varepsilon - \frac{a}{2}\varepsilon\theta_y, \quad \varepsilon_{yy} = \varepsilon\theta_y^2 - \frac{a^2}{2}\varepsilon + \frac{a}{2}\varepsilon\theta_y, \quad \varepsilon\theta_{xx} = -2\varepsilon_x\theta_x + \frac{a}{2}\varepsilon_y, \quad \varepsilon\theta_{yy} = -2\varepsilon_y\theta_y - \frac{a}{2}\varepsilon_y. \tag{C11}$$

Similarly by using

$$\sum_R R_x R_y e^{-ik\cdot R} = -\frac{\partial^2}{\partial k_x \partial k_y}|\gamma_k|e^{i\theta} = -i\frac{a}{2}\frac{\partial}{\partial k_x}|\gamma_k|e^{i\theta}, \tag{C12}$$

we obtain

$$\varepsilon_{xy} = \varepsilon\theta_x\theta_y - \frac{a}{2}\varepsilon\theta_x, \quad \varepsilon\theta_{xy} = -\varepsilon_x\theta_y - \varepsilon_y\theta_x + \frac{a}{2}\varepsilon_x. \tag{C13}$$

APPENDIX D: EACH CONTRIBUTION OF χ

In the present case, the Landau-Peierls contribution simply becomes Eq. (38). Next, the l'-summation in χ_{inter} is carried out in Appendix E, and the result is given by

$$\begin{aligned}
\chi_{inter} = \frac{e^2}{\hbar^2}\sum f(\pm E) \\
\times\Bigg[\left(\frac{\hbar^2}{16m} \pm \frac{\varepsilon^2}{4E}\langle y^2\rangle \pm \frac{\hbar^2}{8m}\frac{s\varepsilon^2}{Et}\right)\theta_x^2 + \frac{\hbar^2}{4m}\left(\eta_x^2 \pm \frac{s\Delta}{Et}\eta_x\varepsilon_x\right) \pm E\langle y^2\rangle\eta_x^2 \\
\pm \frac{\eta_x^2}{4E}(\varepsilon\varepsilon_{yy} + \Delta\Delta_{yy}) \mp \frac{\eta_x\eta_y}{4E}(\varepsilon\varepsilon_{xy} + \Delta\Delta_{xy}) \pm \frac{\theta_x^2}{16E}(\varepsilon\varepsilon_{yy} - \Delta\Delta_{yy}) \mp \frac{\theta_x\theta_y}{16E}(\varepsilon\varepsilon_{xy} - \Delta\Delta_{xy}) \\
\pm \frac{\theta_x^2}{4E}(\Delta\varepsilon_y\eta_y - E^2\eta_y^2) \mp \frac{\theta_x\theta_y}{4E}(\Delta\varepsilon_x\eta_y - E^2\eta_x\eta_y) \mp \frac{\varepsilon\Delta}{4E}(\eta_x\theta_x\theta_{yy} - \eta_x\theta_y\theta_{xy})\Bigg] + (x \leftrightarrow y) + O(s^2). \tag{D1}
\end{aligned}$$

For χ_{FS}, we multiply the Hermitian conjugate of Eq. (B24) by $\frac{\partial u_{k\sigma}^{\pm}}{\partial k_y}$ and integrate the product. Then, with the help of (F7) and (F8), we obtain

$$
\chi_{FS} = \frac{e^2}{2\hbar^2} \sum_{\pm k\sigma} f'(\pm E) \Bigg[\frac{\hbar^2}{2m} \frac{s\varepsilon}{2tE} \varepsilon_x E_x + \frac{\varepsilon^2 E_x}{4E} (\theta_y \theta_{xy} - \theta_x \theta_{yy}) + \frac{\Delta E_x}{4E} \left(\Delta_x \theta_y^2 - \Delta_y \theta_x \theta_y \right)
$$
$$
+ \frac{E_x}{2E} \{ \eta_y (\Delta \varepsilon_{xy} - \varepsilon \Delta_{xy}) - \eta_x (\Delta \varepsilon_{yy} - \varepsilon \Delta_{yy}) \} + E_x^2 \left(\langle y^2 \rangle + \frac{1}{4} \theta_y^2 \right) - \frac{1}{4} E_x E_y \theta_x \theta_y + (x \leftrightarrow y) \Bigg]
$$
$$
+ \frac{e^2}{2\hbar^2} \sum_{\pm k\sigma} f'(\pm E) \frac{\hbar^2}{m} \frac{\Delta}{2E} \sigma (E_x \theta_y - E_y \theta_x) + O(s^2), \tag{D2}
$$

where we have used the relation in Eqs. (C3) and (C4). The last term in Eq. (D2) comes from the contribution of the Zeeman term. We find that it is convenient to make partial integrations in the last three terms, which will be included in χ_1, χ_2, and χ_{OZ} in the main text. With the partial integrations, we obtain

$$
\chi_{FS} = \frac{e^2}{2\hbar^2} \sum_{\pm k\sigma} f'(\pm E) \Bigg[\frac{\hbar^2}{2m} \frac{s\varepsilon}{2tE} \varepsilon_x E_x + \frac{\varepsilon^2 E_x}{4E} (\theta_y \theta_{xy} - \theta_x \theta_{yy}) + \frac{\Delta E_x}{4E} \left(\Delta_x \theta_y^2 - \Delta_y \theta_x \theta_y \right)
$$
$$
+ \frac{E_x}{2E} \{ \eta_y (\Delta \varepsilon_{xy} - \varepsilon \Delta_{xy}) - \eta_x (\Delta \varepsilon_{yy} - \varepsilon \Delta_{yy}) \} + (x \leftrightarrow y) \Bigg]
$$
$$
- \frac{e^2}{2\hbar^2} \sum_{\pm k\sigma} f(\pm E) \Bigg[\pm E_{xx} \left(\langle y^2 \rangle + \frac{1}{4} \theta_y^2 \right) \mp \frac{1}{4} E_{xy} \theta_x \theta_y \mp \frac{1}{4} \left(E_x \theta_x \theta_{yy} - E_x \theta_y \theta_{xy} \right) + (x \leftrightarrow y) \Bigg]
$$
$$
\mp \frac{e^2}{2\hbar^2} \sum_{\pm k\sigma} f(\pm E) \frac{\hbar^2}{m} \sigma \left\{ \left(\frac{\Delta_x}{2E} - \frac{\Delta E_x}{2E^2} \right) \theta_y - \left(\frac{\Delta_y}{2E} - \frac{\Delta E_y}{2E^2} \right) \theta_x \right\} + O(s^2), \tag{D3}
$$

χ_{FS-P} is directly obtained by substituting $M_{\pm\pm\sigma}$ as

$$
\chi_{FS-P} = - \sum_{\pm, k, \sigma} f'(\pm E) \Bigg[\frac{e^2}{4\hbar^2} (\Delta_x \theta_y - \Delta_y \theta_x)^2 + \frac{e^2}{2m} \sigma (\Delta_x \theta_y - \Delta_y \theta_x) + \frac{e^2 \hbar^2}{4m^2} \sigma^2 \Bigg] + O(s^2). \tag{D4}
$$

Using the integration formulas (F3) in Appendix B, we obtain χ_{occ1} as

$$
\chi_{occ1} = -\frac{e^2}{4\hbar^2} \sum_{\pm k\sigma} f(\pm E) \Bigg[\pm E_{xy} \left(\frac{1}{4} \theta_x \theta_y + \eta_x \eta_y \right) + \left(\frac{\hbar^2}{m} \mp E_{xx} \right) \left(\langle y^2 \rangle + \frac{1}{4} \theta_y^2 + \eta_y^2 \right) \mp \frac{\hbar^2}{m} \frac{\varepsilon}{E} \operatorname{Re} X_{yy} \Bigg] + (x \leftrightarrow y) + O(s^2). \tag{D5}
$$

Finally, χ_{occ2} becomes

$$
\chi_{occ2} = \frac{e^2}{\hbar^2} \sum_{\pm, k, \sigma} f(\pm E) \Bigg[\mp \frac{\varepsilon}{2E} \left\{ \theta_x^2 \Delta_y \eta_y - \theta_x \theta_y \Delta_x \eta_y + (x \leftrightarrow y) \right\} \pm \frac{\hbar^2}{2m} \frac{\varepsilon}{E} \sigma (\theta_x \eta_y - \theta_y \eta_x) \Bigg] + O(s^2). \tag{D6}
$$

In the total of these contributions, some terms cancel with each other. In the zeroth order of s (s^0), there are terms proportional to $\frac{\hbar^2}{m} \langle y^2 \rangle$ and $\frac{\hbar^2}{m} \theta_x^2$ in χ_{occ1} and χ_{inter}. However, the latter cancels with each other and only the former appearing in χ_{occ1} contributes to the total susceptibility in the zeroth order. In the previous paper [24], we call this contribution as "intraband atomic diamagnetism," which is shown as χ_{atomic} in Eq. (41).

Collecting the contributions proportional to $\hbar^2/m$ and $\langle y^2 \rangle$ and using integration by parts for terms in χ_{FS}, we obtain

$$
\chi_2 = \frac{e^2}{\hbar^2} \sum_{\pm, k, \sigma} f(\pm E) \Bigg[\mp \frac{\langle y^2 \rangle}{4E} \left(\varepsilon \varepsilon_{xx} + \Delta \Delta_{xx} - \varepsilon^2 \theta_x^2 \right) \mp \frac{\hbar^2}{4m} \left(\frac{s\varepsilon}{2Et} (\varepsilon_{xx} - \varepsilon \theta_x^2) - \frac{\varepsilon}{E} \operatorname{Re} X_{yy} \right) \Bigg] + (x \leftrightarrow y) + O(s^2), \tag{D7}
$$

where we have used the relations of Eqs. (C1) and (C5). Finally, when we use the relation Eq. (C11), we obtain Eq. (43). The last term in χ_{FS-P} is the usual Pauli paramagnetism, Eq. (39). The orbital-Zeeman (OZ) cross terms are characterized by the presence of σ since they are the cross terms of the vector potential and the Zeeman term. They appear in χ_{FS}, χ_{FS-P}, and χ_{occ2} their total becomes Eq. (40).

Note that, in the previous study [21], we derived an expression for χ_{OZ},

$$
\chi_{OZ} = \frac{2e\mu_B}{\hbar} \sum_{\pm, k\sigma} f(E_{k\sigma}^{\pm}) \sigma \Omega_{\pm\sigma} + \frac{i|e|\mu_B}{\hbar} \sum_{lk\sigma} \sigma f'(\pm E) \left\{ \int \frac{\partial u_{k\sigma}^{\pm *}}{\partial k_x} (\pm E - H_k) \frac{\partial u_{k\sigma}^{\pm}}{\partial k_y} d\mathbf{r} - (x \leftrightarrow y) \right\}, \tag{D8}
$$

which yields the same result as Eq. (40) as shown in the following. Using the conjugate of the relation Eq. (B18), the second term of Eq. (D8) is rewritten as

$$
i \sum_{\pm k\sigma} \sigma f'(\pm E) \left\{ \mp E_x \int u^{\pm*}_{k\sigma} \frac{\partial u^{\pm}_{k\sigma}}{\partial k_y} d\mathbf{r} \pm E_y \int u^{\pm*}_{k\sigma} \frac{\partial u^{\pm}_{k\sigma}}{\partial k_x} d\mathbf{r} + \int u^{\pm*}_{k\sigma} \left(\frac{\partial H_k}{\partial k_x} \frac{\partial u^{\pm}_{k\sigma}}{\partial k_y} - \frac{\partial H_k}{\partial k_y} \frac{\partial u^{\pm}_{k\sigma}}{\partial k_x} \right) d\mathbf{r} \right\}.
\tag{D9}
$$

From formula (F1) and Eq. (B25), we obtain Eq. (40) again.

The remaining terms lead to Eq. (42).

APPENDIX E: l' SUMMATION in χ_{inter}

To carry out the summation in χ_{inter} Eq. (25), we first consider the case of $l' = \mp$. From (F2) and (F8), we have

$$
M^z_{\pm\mp\sigma} = \mp \frac{e}{2\hbar} \Delta (\eta_x \theta_y - \eta_y \theta_x),
\tag{E1}
$$

where we have used a relation Eq. (C3). Then, we have

$$
-2 \sum_{\pm,k,\sigma} \frac{f(\pm E)}{(\pm E) - (\mp E)} |M^z_{\pm\mp\sigma}|^2 = -\frac{e^2}{2\hbar^2} \sum_{\pm,k,\sigma} f(\pm E) \left[\pm \frac{\Delta^2}{2E} (\eta_x \theta_y - \eta_y \theta_x)^2 \right].
\tag{E2}
$$

Next, we consider the case of $l' \neq \pm, \mp$. In this case, using Eq. (B24) we can rewrite $M^z_{\pm l'\sigma}$ as

$$
M^z_{\pm l'\sigma} = -\frac{ie}{2\hbar} \left[A_x(\pm E - E_{l'}) \int \frac{\partial u^{\pm*}_{k\sigma}}{\partial k_y} u_{l'k\sigma} d\mathbf{r} + B_x(\mp E - E_{l'}) \int \frac{\partial u^{\mp*}_{k\sigma}}{\partial k_y} u_{l'k\sigma} d\mathbf{r} \pm E_y \int \frac{\partial u^{\pm*}_{k\sigma}}{\partial k_x} u_{l'k\sigma} d\mathbf{r} \right] - (x \leftrightarrow y),
\tag{E3}
$$

where

$$
A_\mu = \mp i \frac{\Delta}{2E} \theta_\mu \pm \frac{s}{2t} \frac{\varepsilon}{E} \varepsilon_\mu, \quad B_\mu = -i \frac{\varepsilon}{2E} \theta_\mu \mp \eta_\mu \mp i \frac{s\varepsilon}{2t} \theta_\mu - \frac{s}{2t} \frac{\Delta}{E} \varepsilon_\mu,
\tag{E4}
$$

for $\mu = x, y$. Then, $M^z_{\pm l'\sigma}$ can be rewritten as

$$
M^z_{\pm l'\sigma} = (M^{xy}_1 + M^{xy}_2) - (x \leftrightarrow y),
\tag{E5}
$$

with

$$
M^{\mu\nu}_1 \equiv -\frac{ie}{2\hbar} \{ A_\mu(\pm E - E_{l'}) \mp E_\mu \} \int \frac{\partial u^{\pm*}_{k\sigma}}{\partial k_\nu} u_{l'k\sigma} d\mathbf{r}, \quad M^{\mu\nu}_2 \equiv -\frac{ie}{2\hbar} \{ B_\mu(\pm E - E_{l'}) \mp 2E B_\mu \} \int \frac{\partial u^{\mp*}_{k\sigma}}{\partial k_\nu} u_{l'k\sigma} d\mathbf{r}.
\tag{E6}
$$

Using these abbreviations, $|M^z_{\pm l'\sigma}|^2$ becomes

$$
|M^z_{\pm l'\sigma}|^2 = |M^{xy}_1|^2 + |M^{xy}_2|^2 + (M^{xy}_1 M^{xy*}_2 + \text{c.c.}) - M^{xy}_1 M^{yx*}_1 - M^{xy}_2 M^{yx*}_2 - (M^{xy}_1 M^{yx*}_2 + \text{c.c.}) + (x \leftrightarrow y).
\tag{E7}
$$

Thus, we need to calculate the six types of matrix elements. In these calculations, we can write the l' summation in a form,

$$
\sum_{l' \neq \pm, \mp} \frac{(\pm E - E_{l'})^n}{\pm E - E_{l'}} \int X^* u_{l'k\sigma} d\mathbf{r} \int u^*_{l'k\sigma} Y d\mathbf{r},
\tag{E8}
$$

with $n = 0, 1$, and 2, and

$$
X, Y = \frac{\partial u^{\pm}_{k\sigma}}{\partial k_\mu}, \frac{\partial u^{\mp}_{k\sigma}}{\partial k_\nu}, \quad \text{etc.}
\tag{E9}
$$

We can carry out these l' summation in the following ways:

(a) $n = 0$ case:

The denominator $\pm E - E_{l'}$ is in the zeroth order with respect to s, and the numerator is in the second order of s because the prefactors E_μ and EB_μ are both in the order of $O(s)$. Therefore, we can neglect this contribution of $n = 0$ in the calculation in the order of $O(s)$.

(b) $n = 1$ case:

Using the completeness condition, $\sum_{l'} u_{l'}(\mathbf{r}) u^*_{l'}(\mathbf{r}') = \delta(\mathbf{r} - \mathbf{r}')$, we obtain

$$
\sum_{l' \neq \pm, \mp} \int X^* u_{l'} d\mathbf{r} \int u^*_{l'} Y d\mathbf{r} = \int X^* Y d\mathbf{r} - \int X^* u^{\pm}_{k\sigma} d\mathbf{r} \int u^{\pm*}_{k\sigma} Y d\mathbf{r} - \int X^* u^{\mp}_{k\sigma} d\mathbf{r} \int u^{\mp*}_{k\sigma} Y d\mathbf{r}.
\tag{E10}
$$

(c) $n = 2$ case:

(a) $\Delta_0/t = 1/4$, $t_2/t = 0.0495 (\simeq \sqrt{3}/36)$
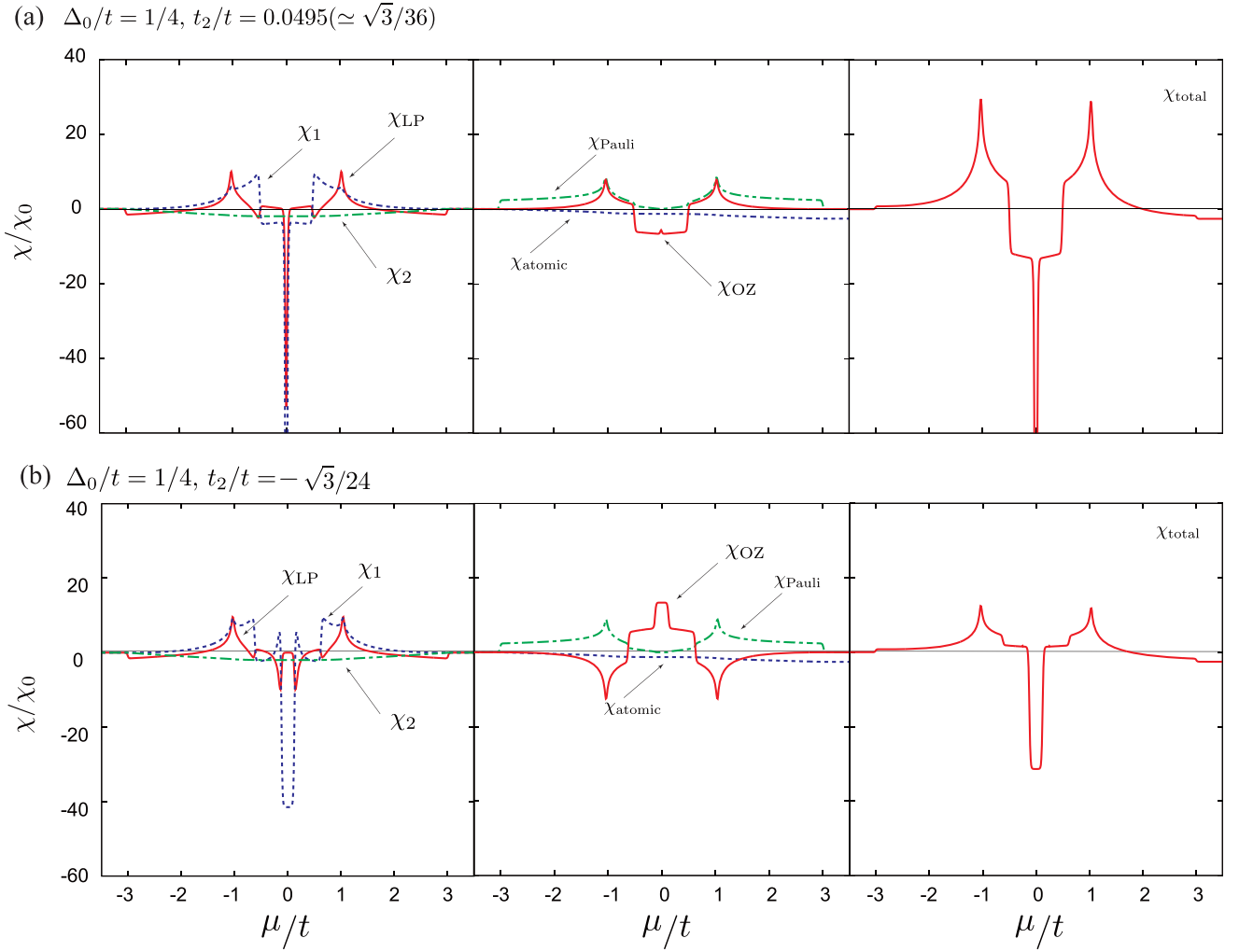

(b) $\Delta_0/t = 1/4$, $t_2/t = -\sqrt{3}/24$

FIG. 9. Each contributions to the magnetic susceptibility as a function of the chemical potential. Left: χ_{LP} (red, solid line), χ_1 (blue, dashed line), and χ_2 (green, dot-dashed line). Middle: χ_{OZ} (red, solid line), χ_{atomic} (blue, dashed line), and χ_{Pauli} (green, dot-dashed line). Right: figures show the total contribution χ_{total}.

Similarly, using the completeness condition,

$$\sum_{l' \neq \pm, \mp} \frac{(\pm E - E_{l'})^2}{\pm E - E_{l'}} \int X^* u_{l'} d\boldsymbol{r} \int u_{l'}^* Y d\boldsymbol{r} = \sum_{l' \neq \pm, \mp} \int X^* (\pm E - H_{\boldsymbol{k}\sigma}) u_{l'} d\boldsymbol{r} \int u_{l'}^* Y d\boldsymbol{r}$$

$$= \int X^* (\pm E - H_{\boldsymbol{k}\sigma}) Y d\boldsymbol{r} \mp 2E \int X^* u_{\boldsymbol{k}\sigma}^{\mp} d\boldsymbol{r} \int u_{\boldsymbol{k}\sigma}^{\mp *} Y d\boldsymbol{r}. \tag{E11}$$

Using formulas (F1)–(F8), (B18), (E10), and (E11), we can carry out the summation of all the combinations as follows:

$$\sum_{l' \neq \pm, \mp} \frac{|M_1^{xy}|^2}{\pm E - E_{l'}} = \frac{e^2}{4\hbar^2} \left[|A_x|^2 \left\{ -\frac{\hbar^2}{2m} \pm \frac{1}{2} E_{yy} \mp \frac{\varepsilon^2}{2E} \theta_y^2 \mp 2E \eta_y^2 \right\} \mp 2E_x \text{Re}[A_x] \langle y^2 \rangle + O(s^2) \right], \tag{E12}$$

$$\sum_{l' \neq \pm, \mp} \frac{|M_2^{xy}|^2}{\pm E - E_{l'}} = \frac{e^2}{4\hbar^2} \left[|B_x|^2 \left\{ -\frac{\hbar^2}{2m} \mp \frac{1}{2} E_{yy} \pm \frac{\varepsilon^2}{2E} \theta_y^2 \pm 2E \eta_y^2 \mp 2E \langle y^2 \rangle \right\} + O(s^2) \right], \tag{E13}$$

$$\sum_{l' \neq \pm, \mp} \frac{M_1^{xy} M_2^{xy*}}{\pm E - E_{l'}} = \frac{e^2}{4\hbar^2} \left[A_x B_x^* \left\{ \mp \frac{i}{2} (2\varepsilon_y \theta_y + \varepsilon \theta_{yy}) - \frac{1}{2E} \left(\Delta \varepsilon_{yy} - \varepsilon \Delta_{yy} - \varepsilon \Delta \theta_y^2 \right) \right\} + O(s^2) \right], \tag{E14}$$

$$\sum_{l' \neq \pm, \mp} \frac{M_1^{xy} M_1^{yx*}}{\pm E - E_{l'}} = \frac{e^2}{4\hbar^2} \left[\pm A_x A_y^* \left(\frac{1}{2} E_{xy} - \frac{\varepsilon^2}{2E} \theta_x \theta_y - 2E \eta_x \eta_y \right) + O(s^2) \right], \tag{E15}$$

$$\sum_{l'\neq\pm,\mp} \frac{M_2^{xy}M_2^{yx*}}{\pm E - E_{l'}} = \frac{e^2}{4\hbar^2}\left[\mp B_x B_y^*\left(\frac{1}{2}E_{xy} - \frac{\varepsilon^2}{2E}\theta_x\theta_y - 2E\eta_x\eta_y\right) + O(s^2)\right],$$

(E16)

$$\sum_{l'\neq\pm,\mp} \frac{M_1^{xy}M_2^{yx*}}{\pm E - E_{l'}} = \frac{e^2}{4\hbar^2}\left[A_x B_y^*\left\{\mp\frac{i}{2}(\varepsilon_x\theta_y + \varepsilon_y\theta_x + \varepsilon\theta_{xy}) - \frac{1}{2E}(\Delta\varepsilon_{xy} - \varepsilon\Delta_{xy} - \varepsilon\Delta\theta_x\theta_y)\right\} + O(s^2)\right].$$

(E17)

Here we have used the relation in Eq. (C4). Then, substituting A_μ and B_μ, and keeping the terms up to the order of $O(s)$, we obtain Eq. (D1).

APPENDIX F: NUMERICAL RESULTS FOR EXTENDED PARAMETERS

Figure 9 shows each contribution to magnetic susceptibility for some choices of parameters near the critical point and negative t_2: $\{\Delta_0/t, t_2/t\}$ = (a) $\{1/4, 0.0495(\simeq \sqrt{3}/36)\}$ and (b) $\{1/4, -\sqrt{3}/24\}$. In case (a), there are two gapless Dirac and two massive Dirac dispersions for two valleys and two spins. The behavior is like a superposition of that in graphene and boron nitride. In particular, in χ_1, the largest flat peak observed for other parameters becomes a sharp peak at $\mu = 0$. This is the behavior known for graphene. We also find χ_{OZ} has the half-quantized value, which is because the system is not an insulator.

In case (b), the system is topologically nontrivial but the spin Chern number is different from the case shown in Fig. 3(c). We find positive value in the gap and negative peak at the van Hove singularities. In cases (a) and (b), the sum rule $\int \chi_{OZ}d\mu = 0$ is confirmed.

[1] F. D. M. Haldane, Model for a Quantum Hall Effect without Landau Levels: Condensed-Matter Realization of the "Parity Anomaly," Phys. Rev. Lett. **61**, 2015 (1988).

[2] C. L. Kane and E. J. Mele, Quantum Spin-Hall Effect in Graphene, Phys. Rev. Lett. **95**, 226801 (2005).

[3] C. L. Kane and E. J. Mele, Z_2 Topological Order and the Quantum Spin-Hall Effect, Phys. Rev. Lett. **95**, 146802 (2005).

[4] B. A. Bernevig and S.-C. Zhang, Quantum Spin-Hall Effect, Phys. Rev. Lett. **96**, 106802 (2006).

[5] B. A. Bernevig, T. L. Hughes, and S.-C. Zhang, Quantum spin-Hall effect and topological phase transition in HgTe quantum wells, Science **314**, 1757 (2006).

[6] M.-F. Yang and M.-C. Chang, Středa-like formula in the spin-Hall effect, Phys. Rev. B **73**, 073304 (2006).

[7] S. Murakami, Quantum Spin-Hall Effect and Enhanced Magnetic Response by Spin-Orbit Coupling, Phys. Rev. Lett. **97**, 236805 (2006).

[8] M. König, S. Wiedmann, C. Brüne, A. Roth, H. Buhmann, L. W. Molenkamp, X.-L. Qi, and S.-C. Zhang, Quantum spin-Hall insulator state in HgTe quantum wells, Science **318**, 766 (2007).

[9] A. Roth, C. Brüne, H. Buhmann, L. W. Molenkamp, J. Maciejko, X.-L. Qi, and S.-C. Zhang, Nonlocal transport in the quantum spin-Hall state, Science **325**, 294 (2009).

[10] C. Brüne, A. Roth, H. Buhmann, E. M. Hankiewicz, L. W. Molenkamp, J. Maciejko, X.-L. Qi, and S.-C. Zhang, Spin polarization of the quantum spin-Hall edge states, Nat. Phys. **8**, 485 (2012).

[11] I. Knez, R.-R. Du, and G. Sullivan, Evidence for Helical Edge Modes in Inverted InAs/GaSb Quantum Wells, Phys. Rev. Lett. **107**, 136603 (2011).

[12] I. Knez, R.-R. Du, and G. Sullivan, Andreev Reflection of Helical Edge Modes in InAs/GaSb Quantum Spin-Hall Insulator, Phys. Rev. Lett. **109**, 186603 (2012).

[13] L. Fu and C. L. Kane, Topological insulators with inversion symmetry, Phys. Rev. B **76**, 045302 (2007).

[14] D. Hsieh, D. Qian, L. Wray, Y. Xia, Y. S. Hor, R. J. Cava, and M. Z. Hasan, A topological Dirac insulator in a quantum spin-Hall phase, Nature (London) **452**, 970 (2008).

[15] R. Nakai and K. Nomura, Crossed responses of spin and orbital magnetism in topological insulators, Phys. Rev. B **93**, 214434 (2016).

[16] Y. Tserkovnyak, D. A. Pesin, and D. Loss, Spin and orbital magnetic response on the surface of a topological insulator, Phys. Rev. B **91**, 041121(R) (2015).

[17] M. Koshino and I. F. Hizbullah, Magnetic susceptibility in three-dimensional nodal semimetals, Phys. Rev. B **93**, 045201 (2016).

[18] H. Suzuura and T. Ando, Theory of magnetic response in two-dimensional giant Rashba system, Phys. Rev. B **94**, 085303 (2016).

[19] Y. Ominato, S. Tatsumi, and K. Nomura, Spin-orbit crossed susceptibility in topological Dirac semimetals, Phys. Rev. B **99**, 085205 (2019).

[20] T. Aftab and K. Sabeeh, Anisotropic magnetic response of Weyl semimetals in a topological insulator multilayer, J. Appl. Phys. **127**, 163905 (2020).

[21] S. Ozaki and M. Ogata, Universal quantization of the magnetic susceptibility jump at a topological phase transition, Phys. Rev. Res. **3**, 013058 (2021).

[22] M. Ogata and H. Fukuyama, Orbital magnetism of Bloch electrons. I. General formula, J. Phys. Soc. Jpn. **84**, 124708 (2015).

[23] M. Ogata, Orbital magnetism of Bloch electrons: II. Application to single-band models and corrections to Landau–Peierls susceptibility, J. Phys. Soc. Jpn. **85**, 064709 (2016).

[24] M. Ogata, Orbital magnetism of bloch electrons: III. Application to graphene, J. Phys. Soc. Jpn. **85**, 104708 (2016).

[25] P.-O. Löwdin, On the non-orthogonality problem connected with the use of atomic wave functions in the theory of molecules and crystals, J. Chem. Phys. **18**, 365 (1950).

[26] H. Matsuura and M. Ogata, Theory of orbital susceptibility in the tight-binding model: Corrections to the Peierls phase, J. Phys. Soc. Jpn. **85**, 074709 (2016).

[27] L. Landau, Diamagnetismus der metalle, Z. Phys. **64**, 629 (1930).

[28] R. Peierls, Zur theorie des diamagnetismus von leitungselektronen, Z. Phys. **80**, 763 (1933).

[29] H. Fukuyama and R. Kubo, Interband effects on magnetic susceptibility. II. Diamagnetism of bismuth, J. Phys. Soc. Jpn. **28**, 570 (1970).

[30] J. Hebborn and E. Sondheimer, The diamagnetism of conduction electrons in metals, J. Phys. Chem. Solids **13**, 105 (1960).

[31] E. I. Blount, Bloch electrons in a magnetic field, Phys. Rev. **126**, 1636 (1962).

[32] J. E. Hebborn, J. M. Luttinger, E. H. Sondheimer, and P. J. Stiles, J. Phys. Chem. Solids **25**, 741 (1964).

[33] H. Fukuyama, Theory of orbital magnetism of Bloch electrons: Coulomb interactions, Prog. Theor. Phys. **45**, 704 (1971).

[34] G. Gómez-Santos and T. Stauber, Measurable Lattice Effects on the Charge and Magnetic Response in Graphene, Phys. Rev. Lett. **106**, 045504 (2011).

[35] A. Raoux, F. Piéchon, J.-N. Fuchs, and G. Montambaux, Orbital magnetism in coupled-bands models, Phys. Rev. B **91**, 085120 (2015).

[36] M. Ogata, Theory of magnetization in Bloch electron systems, J. Phys. Soc. Jpn. **86**, 044713 (2017).

[37] M. Ezawa, A topological insulator and helical zero mode in silicene under an inhomogeneous electric field, New J. Phys. **14**, 033003 (2012).

[38] M. Ezawa, Topological phase transition and electrically tunable diamagnetism in silicene, Eur. Phys. J. B **85**, 363 (2012).

[39] G. G. Guzmán-Verri and L. C. Lew Yan Voon, Electronic structure of silicon-based nanostructures, Phys. Rev. B **76**, 075131 (2007).

[40] C.-C. Liu, H. Jiang, and Y. Yao, Low-energy effective Hamiltonian involving spin-orbit coupling in silicene and two-dimensional germanium and tin, Phys. Rev. B **84**, 195430 (2011).

[41] C.-C. Liu, W. Feng, and Y. Yao, Quantum Spin-Hall Effect in Silicene and Two-Dimensional Germanium, Phys. Rev. Lett. **107**, 076802 (2011).

[42] L. M. Roth, B. Lax, and S. Zwerdling, Theory of optical magneto-absorption effects in semiconductors, Phys. Rev. **114**, 90 (1959).

[43] C.-X. Liu, X.-L. Qi, H. J. Zhang, X. Dai, Z. Fang, and S.-C. Zhang, Model Hamiltonian for topological insulators, Phys. Rev. B **82**, 045122 (2010).

[44] J. C. Slater, Atomic shielding constants, Phys. Rev. **36**, 57 (1930).

[45] S. Blundell, *Magnetism in Condensed Matter* (Oxford University Press, Oxford, UK, 2001).

[46] D. N. Sheng, Z. Y. Weng, L. Sheng, and F. D. M. Haldane, Quantum Spin-Hall Effect and Topologically Invariant Chern Numbers, Phys. Rev. Lett. **97**, 036808 (2006).

[47] A. Raoux, M. Morigi, J.-N. Fuchs, F. Piéchon, and G. Montambaux, From Dia- to Paramagnetic Orbital Susceptibility of Massless Fermions, Phys. Rev. Lett. **112**, 026402 (2014).

[48] A. Gutiérrez-Rubio, T. Stauber, G. Gómez-Santos, R. Asgari, and F. Guinea, Orbital magnetic susceptibility of graphene and MoS$_2$, Phys. Rev. B **93**, 085133 (2016).

[49] F. Piéchon, A. Raoux, J.-N. Fuchs, and G. Montambaux, Geometric orbital susceptibility: Quantum metric without Berry curvature, Phys. Rev. B **94**, 134423 (2016).

[50] M. Koshino and T. Ando, Anomalous orbital magnetism in Dirac-electron systems: Role of pseudospin paramagnetism, Phys. Rev. B **81**, 195431 (2010).

[51] D. Xiao, M.-C. Chang, and Q. Niu, Berry phase effects on electronic properties, Rev. Mod. Phys. **82**, 1959 (2010).

[52] T. Thonhauser, Theory of orbital magnetization in solids, Int. J. Mod. Phys. B **25**, 1429 (2011).

[53] G. Sundaram and Q. Niu, Wave-packet dynamics in slowly perturbed crystals: Gradient corrections and Berry-phase effects, Phys. Rev. B **59**, 14915 (1999).

[54] D. Xiao, J. Shi, and Q. Niu, Berry Phase Correction to Electron Density of States in Solids, Phys. Rev. Lett. **95**, 137204 (2005).

[55] T. Thonhauser, D. Ceresoli, D. Vanderbilt, and R. Resta, Orbital Magnetization in Periodic Insulators, Phys. Rev. Lett. **95**, 137205 (2005).

[56] D. Ceresoli, T. Thonhauser, D. Vanderbilt, and R. Resta, Orbital magnetization in crystalline solids: Multiband insulators, Chern insulators, and metals, Phys. Rev. B **74**, 024408 (2006).

[57] J. Shi, G. Vignale, D. Xiao, and Q. Niu, Quantum Theory of Orbital Magnetization and its Generalization to Interacting Systems, Phys. Rev. Lett. **99**, 197202 (2007).

[58] X. Qian, J. Liu, L. Fu, and J. Li, Quantum spin-Hall effect in two-dimensional transition metal dichalcogenides, Science **346**, 1344 (2014).

[59] Z. Fei, T. Palomaki, S. Wu, W. Zhao, X. Cai, B. Sun, P. Nguyen, J. Finney, X. Xu, and D. H. Cobden, Edge conduction in monolayer WTe$_2$, Nat. Phys. **13**, 677 (2017).

[60] S. Tang, C. Zhang, D. Wong, Z. Pedramrazi, H.-Z. Tsai, C. Jia, B. Moritz, M. Claassen, H. Ryu, S. Kahn, J. Jiang, H. Yan, M. Hashimoto, D. Lu, R. G. Moore, C.-C. Hwang, C. Hwang, Z. Hussain, Y. Chen, M. M. Ugeda *et al.*, Quantum spin-Hall state in monolayer 1T′-WTe$_2$, Nat. Phys. **13**, 683 (2017).

[61] Y. Yanase and M. Sigrist, Superconductivity and magnetism in noncentrosymmetric system: Application to CePt$_3$Si, J. Phys. Soc. Jpn. **77**, 124711 (2008).

[62] Y. Yanase and S. Fujimoto, Microscopic theory of pairing mechanisms, in *Noncentrosymmetric Superconductors: Introduction and Overview*, edited by E. Bauer and M. Sigrist (Springer, Berlin, 2012), pp. 171–210